sustainability

MDPI

Article

Optimal Power Flow in Wind–Photovoltaic Energy Regulation Systems Using a Modified Turbulent Water Flow-Based Optimization

Ali S. Alghamdi

Department of Electrical Engineering, College of Engineering, Majmaah University, Al-Majmaah 11952, Saudi Arabia; aalghamdi@mu.edu.sa

Abstract: This paper describes how to obtain optimal power flow (OPF) in power systems that integrate wind turbine (WT) and solar photovoltaic (PV) producers. A modified technique called modified turbulent water flow-based optimization (MTFWO) is presented to solve the nonconvex and nonlinear OPF problem effectively. In the OPF model, power output from renewable sources is regarded as a dependent variable. At the same time, the voltage at the bus terminals of WT/PV is used as a controller (decision variable). The amount of power generated by WT and PV generators is modeled using data collected in real time on the wind speed and the amount of irradiation from the sun. Although the TFWO algorithm has its benefits, it also has certain shortcomings in solving challenging problems. By more effectively searching the feasible space using different interaction mechanisms and improving exploitation capabilities, this paper improves the TFWO algorithm's performance. We compare the performance and effectiveness of the suggested MTFWO method with cutting-edge optimization algorithms for solving the OPF problems, using the same system-specific data, limitations, and control variables in the comparisons.

Keywords: the optimization of turbulence in engineered water flows; power systems; optimum power flow (OPF); renewable energy sources (RES) such as wind and solar; nonconvex cost functions

Citation: Alghamdi, A.S. Optimal Power Flow in Wind–Photovoltaic Energy Regulation Systems Using a Modified Turbulent Water Flow-Based Optimization. *Sustainability* **2022**, *14*, 16444. https://doi.org/10.3390/su142416444

Academic Editor: Ashwin M. Khambadkone

Received: 9 October 2022
Accepted: 23 November 2022
Published: 8 December 2022

1. Introduction

In addition to being a popular power system design tool, optimal power flow (OPF) is an important optimization test problem [1] due to its multidimensional, nonconvex, and nonlinear nature. Over the last few decades, researchers have experimented with a variety of OPF formulations to increase the efficiency of a power grid exposed to a wide range of physical restrictions [1]. To improve the existing condition of affairs, a variety of categories and goals are used. Theoretically, any of the two possible OPF solutions might be implemented [2], each of which has its distinct mathematical characteristics and processing requirements.

The recent interest in OPF optimization challenges [2] may be attributed to the increasing popularity of decentralized energy sources in network applications. Integration of distant and intermittent renewable energy sources such as photovoltaic (PV) systems and wind energy into conventional power networks has posed significant operational and administrative issues [3]. These advancements include solar panels and wind turbines. Solar energy is converted into electricity through PVs. Temperature and solar radiation affect solar energy's ability to generate electricity. As a result, assessing PV system performance in operation is crucial for modeling, managing, and optimizing them in the future. Optimizing the reflector-PV collector configuration allows solar energy to be deployed more efficiently [4,5]. Recognizing the inherent unpredictability of intermittent energy sources such as wind and solar cells is essential for optimizing their use. The unpredictability of renewable resources, which imposes unanticipated dynamics on the power system, has made it far more difficult to find a suitable solution to the OPF problem [6]. Therefore,

photovoltaic solar collectors are usually interconnected with electrical sources or energy accumulators [7].

Linear programming (LP) [8], Newton's method (NM) [8], quadratic programming (QP) [9], and nonlinear programming (NP) [10] all have strong convergence features and may be utilized to address OPF problems. In reality, however, system goal functions are seldom differentiable, smooth, or convex [11]. For instance, it may be challenging to describe the fuel costs of thermal plants as a convex function with all required features using typical approaches [11]. Numerous theories have this characteristic, including piecewise quadratic cost, valve points, and constrained operating ranges [11]. Before agreeing on the ideal solution, it is usual practice to iterate and repeatedly make multiple considerable changes [11].

We need a quicker and more effective solution for genuine OPF instances. Recent research indicates that metaheuristics may be effective for tackling complex optimization problems. Metaheuristics may be used to address such challenges. Given that all metaheuristics have the same underlying constraints, it is straightforward to develop a uniform set of methods to solve them. The following features are shared by several prominent metaheuristics [12]. The following are some instances of AI-based optimization strategies used to handle OPF issues: a grey wolf optimizer (GWO) [13], MHBMO (a modified honey bee mating optimization) [14], a multiobjective glowworm swarm optimization (MOGSO) [15], a new differential evolution (DE) [16], a coronavirus method [17]; an efficient MOEA (multiobjective evolutionary algorithm) [18], a BSA (a bird swarm algorithm) [19], a multiobjective OPF using GWO and DE algorithms [20], a surrogate-assisted multiobjective probabilistic OPF [21], and a symbiotic organisms search (SOS) [22]. Using a modified moth swarm algorithm (MMSA), which considers both direct expenditures and the likelihood of over- or underestimating such costs, it is possible to decrease the operating costs of wind power-producing units [23].

Solving the OPF problem is notoriously challenging due to the nonconvex and nonlinear endeavor. Existing algorithms still need to improve their performance to solve such a complex problem. Mojtaba Ghasemi and colleagues [24] established the notion of optimization based on turbulent water flow (TFWO) in 2021, among others. We create a unique and successful modification of the TFWO (MTFWO) approach to address various OPF problems in hybrid systems. The speed of convergence, finding the optimal solution, and the algorithm's robustness in finding the near-optimal solutions are important factors in determining the algorithm's performance. Moreover, in this paper, the comprehensive comparison of the developed algorithm with existing state-of-the-art methods shows the capability of this algorithm to solve OPF problems.

The main highlights of the paper are:

- Improving the convergence speed, exploration, and exploitation capabilities of the conventional TFWO algorithm;
- Introducing an enhanced operator to update the population to increase the power of local search of the original TFWO algorithm;
- Application of the proposed modified algorithm to solve the nonconvex and nonlinear OPF problems;
- Voltage magnitude at WT and PV buses is considered a decision variable, while WT and PV power generation forecasts are dependent variables in the OPF problem.

This article explains the following: The OPF problem formulation is presented in Section 2. In Section 3, we will explain just how our proposed method might increase productivity. In Section 4, the suggested approach is evaluated on a real IEEE 30-bus network, where numerous load distribution functions are studied, and the final strategy is assessed. Section 5 provides a synopsis of the method's results and conclusions.

2. Problem Formulation

Due to the inherent unpredictability of both processes, merging wind and solar energy makes it more difficult to solve the OPF issue. This article covers the OPF issue, which

explains the variability of WT and PV output under various practical assumptions. These particular hypotheses are detailed below: Due to the impossibility of dispatching the active power production of solar panels and wind turbines, these values are taken into account as anticipated values in the total power factor issue. The OPF is administered carefully at regular intervals of 10 min [25]. When the sampling interval for wind speed and solar irradiance is one minute, there are 10 observations at each t-interval. There have likely been 100 total readings at this time. Using measurement data, probabilistic models of wind speed and solar irradiance, and the mechanical properties of the WT and PV units, it is possible to predict the active power production of wind turbines and photovoltaic units. This allows for more precise measurements of the active power produced by these two types of equipment. In line, the reactive power provided by WT and PV units is between −0.4 and 0.5% of their active power. Consequently, the voltage levels on the PV and WT buses might affect the OPF issue. To illustrate the OPF issue, consider the following mathematical equation [25]:

$$\text{Objective function } (F): \ \text{Min} F(x, y) \tag{1}$$

Subjected to:

$$\text{Inequality constraints } (h): \ h(x, y) \leq 0 \tag{2}$$

$$\text{Equality constraints } (g): \ g(x, y) = 0 \tag{3}$$

$$x \in X \tag{4}$$

$$\text{Control variables}: \ x = \begin{bmatrix} P_{G2}, \ldots, P_{GNG}, V_{G1}, \ldots, V_{GNG}, V_{WT}, V_{PV}, \\ T_1, \ldots, T_{NT}, Q_{C1}, \ldots, Q_{CNC} \end{bmatrix} \tag{5}$$

T_i (i = 1: NT) represents the tap setting on the transformer, Q_{Ci} (i = 1: NC) represents the adjustment to the shunt VAR, and x represents the vector of control variables. F represents the objective function that needs to be minimized, P_{Gi} (i = 1: NG) represents the active power output of the thermal units, and V_{Gi} (i = 1: NG) represents the generator voltage (WT and PV) [25].

$$\text{Dependent variables}: \ y = \begin{bmatrix} P_{G1}, V_{L1}, \ldots, V_{LNL}, Q_{G1}, \ldots, Q_{GNG}, \\ Q_{WT}, V_{PV}, S_{l1}, \ldots, S_{l\,NTL} \end{bmatrix} \tag{6}$$

The current number of power plants, thermal transformers, and variable-frequency-drive (VAR) compensators that are in operation are NG, NT, and NC, respectively. The reactive power outputs from the generator, represented by Q_{Gi} (i = 1: NG); the power on the slack bus, represented by P_{G1}; the voltage at the load bus, represented by V_{Li} (i = 1: NTL); and the transmission line loads make up the components of vector y. Load bus capacity and transmission line count are denoted by NL and NTL, respectively.

2.1. Constraints

The solution to the classical nonlinear OPF equations may be written as (7) and (8), as proven by the inequality limitations (g) in Equation (2).

$$P_{Gi} - P_{Di} - V_i \sum_{j=1}^{NB} V_j \left[G_{ij} * \cos\left(\delta_i - \delta_j\right) + B_{ij} * \sin\left(\delta_i - \delta_j\right) \right] = 0; \ I = 1: \ NB \tag{7}$$

$$Q_{Gi} - Q_{Di} - V_i \sum_{j=1}^{NB} V_j \left[G_{ij} * \sin(\delta_i - \delta_j) - B_{ij} * \cos(\delta_i - \delta_j) \right] = 0; \ i = 1: \ NB \tag{8}$$

In the above equations, Q_{Di} and P_{Di} are the reactive and real load demands, respectively, and NB is the total number of buses. These three variables are represented in the equation by parentheses. The real component of the bus admission matrix is denoted by the letter G_{ij}, while the imaginary component is denoted by the letter B_{ij}. The voltage angle that exists between the i bus and the j bus is represented by $\delta_{ij}\left(= \delta_i - \delta_j\right)$. Equation (3), when applied to the study of the operational variables of a function, demonstrates the existence of inequality boundaries. This category also includes restrictions placed on the

amount of reactive power that can be generated by generators and the amount of branch flow [25].

$$V_{Li}^{\min} \le V_{Li} \le V_{Li}^{\max}; i = 1, 2, \ldots, NL \tag{9}$$

$$Q_{Gi}^{\min} \le Q_{Gi} \le Q_{Gi}^{\max} \tag{10}$$

$$S_{li} \le S_{li}^{\max}; l = 1, 2, \ldots, NTL \tag{11}$$

Constraints (4) define the space of possible solutions for the OPF problem:

$$P_{Gi}^{\min} \le P_{Gi} \le P_{Gi}^{\max}; i = 1, 2, \ldots, N \tag{12}$$

$$V_{Gi}^{\min} \le V_{Gi} \le V_{Gi}^{\max}; i = 1, 2, \ldots, NG \tag{13}$$

$$T_i^{\min} \le T_i \le T_i^{\max}; \forall i = 1, \ldots, NT \tag{14}$$

$$Q_{Ci}^{\min} \le Q_{Ci} \le Q_{Ci}^{\max}; \forall i = 1, \ldots, NC \tag{15}$$

The restrictions that apply to both the independent variable (x) and the other controls (other variables) are the same. In addition to this, the inequality requirements of the dependent variables, particularly y, may be relaxed by including these components in the objective function in the form of quadratic penalty factors. The goal of performing these steps is to narrow down the available choices.

2.2. Objective Functions

One of the primary objectives taken into account while examining OPF competitions for thermal power plants is fuel cost (*Fcost*). The price of a thermal generating unit may be expressed mathematically as a quadratic function of the generator's output power.

$$\text{Min}cost(x, y) = \sum_{i=1}^{N\ G} \left(\alpha_i + b\ _i P_{G\ i} + c_i\ P_{Gi}^2 \right) \tag{16}$$

where P_{Gi} is the active power output of the ith thermal power plant and a_i, b_i, and c_i are the cost coefficients that correlate to that plant's power output. The following aim function has to be met in order to achieve the desired result of minimizing the overall active power loss (*Ploss*) in the system.

$$\text{Min}Ploss(x, y) = \sum_{i=1}^{NTL} \sum_{\substack{j=1 \\ j \ne i}}^{NTL} G_{ij} V_i^2 + B_{ij} V_j^2 - 2 V_i V_j cos\delta_{ij} \tag{17}$$

Safety and service quality may be measured, in large part, by looking at the bus voltage. The primary goal here is to reduce the amount of voltage variation (*VD*) on the load bus, as shown by the following expression:

$$\text{Min}VD(x\ , y) = \sum_{i=1}^{NL} \left| \ V_i - V_i^{ref} \right| \tag{18}$$

where V_i is the bus i voltage standard, which is typically 1 p.u. and indicates the level of voltage present on the ith bus. At a power plant that runs on fossil fuels, such as coal, petroleum, and natural gas, the generation of electricity is accomplished by the combustion of those fuels. When anything is burnt, a significant amount of toxins is discharged into the atmosphere. In the context of this inquiry, the approach [26] is used to calculate emission predictions for both nitrogen oxides (NOx) and sulfur oxides (SOx).

$$\text{Min}Emission\ (x, y) = \sum_{i=1}^{NG} \left(\alpha_i + \beta_i P_{Gi} + \gamma_i P_{Gi}^2 + \xi_i exp(\theta_i P_{Gi} \right) \tag{19}$$

where α_i (ton/h), β_i (ton/h MW), γ_i (ton/h MW2), ξ_i (ton/h), and θ_i (1/MW) are emission coefficients of the ith power plant. The amount of tax for producers can be determined based on the amount of greenhouse gases emitted, making producers use more suitable and renewable fuels, such as wind and solar power plants that produce electric energy, and the amount of environmental pollution from fossil fuels can be reduced effectively. However, a carbon tax is not the only way to consider the externalities associated with conventional energy conversion.

A penalty function is added to the primary objective function in the following way in order to take into account the fact that the restrictions have been broken:

$$J = \sum_{i=1}^{NG} F_i(P_{Gi}) + \lambda_P \left(P_{G1} - P_{G1}^{lim}\right)^2 + \lambda_Q \sum_{i=1}^{NG} \left(Q_{Gi} - Q_{Gi}^{lim}\right)^2 + \lambda_V \sum_{i=1}^{NL} \left(V_{Li} - V_{Li}^{lim}\right)^2 + \lambda_S \sum_{i=1}^{NTL} \left(S_{li} - S_{li}^{lim}\right)^2 \quad (20)$$

where λ_P, λ_V, $\lambda_{Q,}$ and λ_S are the penalty factors; and z^{lim} is a variable that is defined in the following equation as an auxiliary variable:

$$z^{\lim} = \begin{cases} z; \ z^{\min} \le z \le z^{\max} \\ z^{\min}; \quad z \le z^{\min} \\ z^{\max}; \quad z \ge z^{\max} \end{cases} \quad (21)$$

2.3. Modeling of WT and PV Generation

2.3.1. Modeling of WT Generation

When the wind velocity (v) is known, the following equation [25] may be used to calculate the power output of a WT:

$$P_{W\,T}\,(v) = \begin{cases} 0\ v \le \ v_{ci} \\ \frac{v - v_{ci}}{v_n - v_{ci}} P_{w\,tn} v_{ci} \le \ v \le v_n \\ P_{\,wtn} v_n \le v \ \le v_{c\,o} \\ 0\ v \ge v_{c\,o} \end{cases} \quad (22)$$

P_{wtn} is the nominal power, v_n is the wind speed, v_{ci} is the speed at which the wind turbine starts producing electricity, and v_{co} is the speed at which it ceases. Weibull distributions may be used as an overarching framework for characterizing the randomness of wind speed at a given time and location.

$$f_{\,v}\,(v) = \frac{K}{C} * \left(\frac{v}{C}\right)^{K-1} * \ e^{-1*\left(\frac{v}{C}\right)^k}, v > 0 \quad (23)$$

The cumulative density function (CDF) for the Weibull distribution is:

$$F_{\,v}(v) = 1 - Exp(-\left(\frac{v}{C}\right)^k) \quad (24)$$

For the purpose of estimating the v, we have studied the CDF with its inverse:

$$v = C * (-1 * ln\ (r))^{\frac{1}{k}} \quad (25)$$

Weibull's probability density function for wind speed is represented by the symbol $f_v(v)$; the size and shape parameters of the Weibull distribution are represented by the symbols C and k; and r is a uniformly distributed random integer that may take on any value between 0 and 1, respectively. We are able to estimate WT's output power [25] by basing our calculations on the likelihood of all potential states over that time period.

$$P_{\,W\,T} = \frac{\sum_{g=1}^{N_v} P_{W\,Tg} * f_v\left(v_g^t\right)}{\sum_{g=1}^{N_v} f_v\left(v_g^t\right)} \quad (26)$$

where v_g^t is the gth state of wind speed at the tth time interval; P_{WTg} is the power generation of WT calculated using (22) for $v = v_g^t$; $f_v\left(v_g^t\right)$ is the probability of the wind speed for state g during the specified interval t.

2.3.2. Modeling of PV Generation

Solar irradiation is directly related to the amount of electricity that may be extracted from a PV system [25]:

$$P_{PV}(S) = \begin{cases} P_{pvn}\left(\frac{S^2}{R_C S_{stc}}\right) S \leq R_C \\ P_{pvn}\left(\frac{S}{S_{stc}}\right) S \geq R_C \end{cases} \quad (27)$$

The symbol S represents the solar irradiance at the surface of the PV module, whereas the letter S_{stc} represents the solar irradiance under standard test circumstances. P_{pvn} denotes the nominal output power of the PV unit. A certain spectral irradiance value is denoted by the letter sign R_c. One may use beta PDF [25] to build a model that adequately accounts for the stochastic nature of solar irradiation:

$$f_s(S) = \begin{cases} \frac{\Gamma(\alpha+\beta)}{\Gamma(\alpha)\Gamma(\beta)} S^{\alpha+1}(1-S)^{\beta-1}; 0 \leq S \leq 1,\ \alpha \geq 0, \beta \geq 0 \\ 0; \text{Otherwise} \end{cases} \quad (28)$$

In this expression, S represents the kW/m^2 of solar irradiance, $f_s(S)$ is the beta distribution function of S. α, β, and Γ ( ) are the shape parameters and gamma function, respectively.

Predicted PV production power [25] is evaluated in light of the probabilities of all solar irradiance levels across the observed time range.

$$P_{PV} = \frac{\sum_{g=1}^{N_S} P_{PV,g} f_S\left(S_g^t\right)}{\sum_{g=1}^{N_S} f_S\left(S_g^t\right)} \quad (29)$$

where S_g^t represents the gth possible state of solar irradiance at the tth time interval, P_{PVg} represents the power production of PV computed using Equation (27), and $f_S(S_g^t)$ represents the probability of solar irradiance for state g at time t.

3. The Proposed Optimization Algorithm

3.1. TFWO

As was stated at the beginning of the paper, the rest of the research will focus on documenting and recreating the original implementation and performance of the TFWO algorithm at each level.

3.1.1. Formation of Whirlpools

The beginning population, which is denoted by X^0 and Np, the total number of objects, is partitioned into N_{Wh} groups, sometimes known as whirlpools, before the algorithm continues with any further steps. Then, the strongest member of the whirlpool is chosen to be the center and the hole (the population that has the greatest values of the objective function f ( )). This results in a centrifugal force that grows with increasing distance from the center of the whirlpool. As a consequence of this force, objects and particles (X; Np-N_{Wh}: the number of starting objects) are pushed in a direction that is counter to the direction in which they are moving.

3.1.2. The Effects of Whirlpools on Objects and Particles of Its Set and Other Whirlpools

Every whirlpool (Wh) functions as a sucking well or hole. It has the propensity to centralize the positions of its associated objects (X) by applying a centripetal force on them

and plunging them into its well. Centrifugal force is used to achieve this effect. This indicates that the *i*th particle's position (X_i) is combined with that of the *j*th whirlpool's (Wh_j) via the *j*th whirlpool's behavior, making $X_i = Wh_j$.

However, there are still some deviations brought about by extra whirlpools, as determined by their relative positions (*Wh-Whj*) and objective values (f ( ), which cause some deviations (ΔX_i). Figure 1 depicts the impact of these whirlpools on their collection of objects and particles, leading to a new position for the *i*th particle equal to $X_i^{new} = Wh_j - \Delta X_i$. Figure 1 shows how objects and particles travel around their whirlpool's center while keeping their distinct angle (δ).

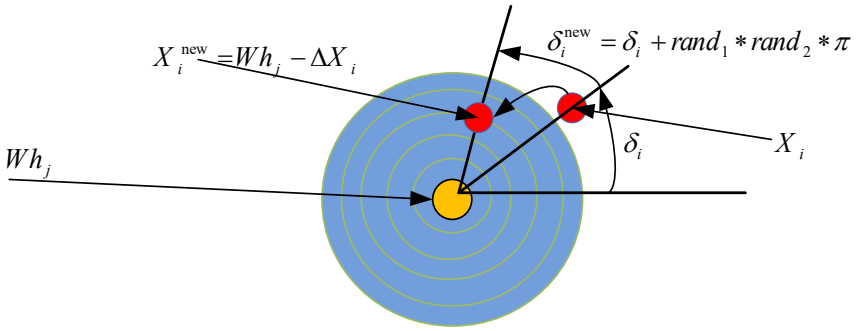

Figure 1. The model by whirlpool for optimization purposes.

So, this angle changes somewhat at each time step (in the algorithm):

$$\delta_i^{\text{new}} = \delta_i + rand_1 * rand_2 * \pi$$

The extreme and intermediate values of Equation (30) for the furthest and nearest whirlpools are used to model and calculate ΔX_i. This allows us to solve for *j*th using Equations (34) and (35) below, where *j*th is the value of the angle of the *i*th particle concerning its whirlpool, i.e., δ_i, the variation of the particle's position that is amenable to reduction.

$$\Delta_t = f(Wh_t) * |\text{sum}(Wh_t) - \text{sum}(X_i)|^{0.5} \tag{30}$$

$$\Delta X_i = (1 + |cos(\delta_i^{\text{new}}) - sin(\delta_i^{\text{new}})|) * \left(cos(\delta_i^{\text{new}}) * \left(Wh_f - X_i\right) - sin(\delta_i^{\text{new}}) * (Wh_w - X_i)\right) \tag{31}$$

$$X_i^{\text{new}} = Wh_j - \Delta X_i \tag{32}$$

where Wh_f is Wh with a minimum value of Δ_t and Wh_w is Wh with a maximum value of Δ_t, respectively.

- Pseudocode 1:

  for $t = 1 : N_{Wh} - \{j\}$

  $$\Delta_t = f(Wh_t) * |\text{sum}(Wh_t) - \text{sum}(X_i)|^{0.5}$$

  end
  $Wh_f = Wh$ with a minimum value of Δ_t
  $Wh_w = Wh$ with a maximum value of Δ_t
  $\delta_i^{\text{new}} = \delta_i + rand_1 * rand_2 * \pi$
  $\Delta X_i = (1 + |cos(\delta_i^{\text{new}}) - sin(\delta_i^{\text{new}})|) * \left(cos(\delta_i^{\text{new}}) * \left(Wh_f - X_i\right) - sin(\delta_i^{\text{new}}) * (Wh_w - X_i)\right)$
  $X_i^{\text{new}} = Wh_j - \Delta X_i$

- Pseudocode 2:

  $X_i^{new} = \min\left(\max\left(X_i^{new}, X^{min}\right), X^{max}\right)$
  if $f\left(X_i^{new}\right) <= f(X_i)$

$$X_i = X_i^{new}$$

$$f(X_i) = f(X_i^{new})$$

end

3.1.3. Centrifugal Force

The moving item feels a pull toward the center as a result of the centripetal force, but it also feels a push away from the center as a result of the centrifugal force. Newton's first rule of motion says that an object at rest will remain at rest, and an object in motion will continue to travel at the same speed and in the same direction unless an unbalanced force acts upon it and causes it to move in a different direction or at a different pace. Sometimes the centrifugal force (FE_i) of the vortex is stronger than the FE_i (also known as the traction force) of the vortex, and this results in the particle being moved to a new place at random. The centrifugal force is modeled in Equation (33) as a random variable along one dimension of the target. This is due to the fact that it happens at random for each aim (or the solution). To accomplish this, first, the FE_i is determined by its angle with the center of the hole (as in Equation (33)), and then, if this force is greater than the random r-value, the centrifugal action is carried out randomly for the pth dimension using Equation (34). To summarize, to accomplish this, first the FE_i is determined by its angle with the center of the hole (as in Equation (33)), and then, to summarize, to accomplish this, the first thing that has to be carried out in order to complete this procedure is to calculate the FE_i. This is performed by calculating the angle of the item in relation to the center of the hole.

$$FE_i = \left[\left(\cos(\delta_i^{\text{new}}) \right)^2 * \left(\sin(\delta_i^{\text{new}}) \right)^2 \right]^2 \tag{33}$$

$$x_{i,p} = x_p^{min} + x_p^{max} - x_{i,p} \tag{34}$$

- Pseudocode 3:

  $FE_i = \left[\left(\cos(\delta_i^{\text{new}}) \right)^2 * \left(\sin(\delta_i^{\text{new}}) \right)^2 \right]^2$

  if $rand < FE_i$

  $p = \text{round}(1 + \text{rand} * (D - 1));$

  $x_{i,p} = x_p^{min} + x_p^{max} - x_{i,p}$

  $f(X_i) = f(X_i^{new})$

  end

  This is expressed as shown in Figure 2.

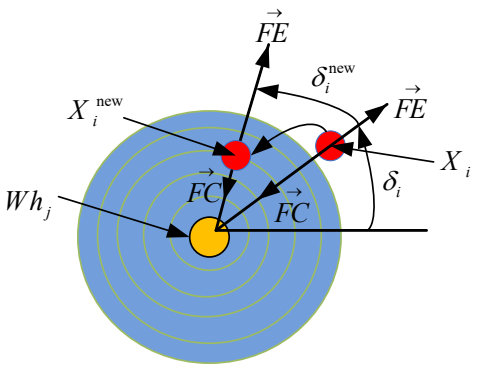

Figure 2. The various types of forces in a whirlpool.

3.1.4. Interactions between the Whirlpools

Their interactions influence the nearby things, which causes them to be tossed about like debris in a tornado. We have attempted to model this phenomenon analogous to how whirlpools influence the movement of things and particles. In this model, individual whirlpools have a gravitational pull on one another, exert centrifugal force on one another, and eventually drag other whirlpools toward their centers. Conceptually, these whirlpools are analogous to vortices, i.e., they unify the position of the considered whirlpool with its position. A little portion of Equation (35) models and calculates *Whj* by searching for the whirlpool closest to the objective function. Then, using the value of the angle of the *j*th whirlpool, *j*, together with the following equations, Equations (36) and (37), we obtain a variation of the whirlpool's position that is amenable to a decrease in the objective function of the whirlpool (artificial intelligence).

$$\Delta_t = f(Wh_t) * \left|\text{sum}(Wh_t) - \text{sum}\left(Wh_j\right)\right| \tag{35}$$

$$\Delta Wh_j = rand(1, D) * \left|\cos\left(\delta_j^{\text{new}}\right) + \sin\left(\delta_j^{\text{new}}\right)\right| * \left(Wh_f - Wh_j\right) \tag{36}$$

$$Wh_j^{\text{new}} = Wh_f - \Delta Wh_j \tag{37}$$

- Pseudocode 4:

  for $t = 1 : N_{Wh} - \{j\}$

  $$\Delta_t = f(Wh_t) * \left|\text{sum}(Wh_t) - \text{sum}\left(Wh_j\right)\right|$$

  end
  $Wh_f = Wh$ with a minimum value of Δ_t
  $Wh_j^{\text{new}} = Wh_f - \Delta Wh_j$
  $\Delta Wh_j = rand(1, D) * \left|\cos\left(\delta_j^{\text{new}}\right) + \sin\left(\delta_j^{\text{new}}\right)\right| * \left(Wh_f - Wh_j\right)$
  $\delta_j^{\text{new}} = \delta_j + rand_1 * rand_2 * \pi$

- Pseudocode 5:

  $Wh_j^{\text{new}} = \min\left(\max\left(Wh_j^{\text{new}}, X^{min}\right), X^{max}()\right)$
  if $f\left(Wh_j^{\text{new}}\right) <= f\left(Wh_j\right)$

  $$Wh_j = Wh_j^{\text{new}}$$
  $$f\left(Wh_j\right) = f\left(Wh_j^{\text{new}}\right)$$

  end

When this happens, the strongest new member of the whirlpool is selected as the new center and hole of the whirlpool for the following iteration. The roles of this strongest new member are replaced with the roles of the previous center and well of the whirlpool, as shown by the following pseudocode:

if $f(X_{best}) <= f\left(Wh_j\right)$

$$Wh_j \leftrightarrow X_{best}$$
$$f\left(Wh_j\right) \leftrightarrow f(X_{best})$$

end

The flowchart of the TFWO optimization method is shown in Figure 3.

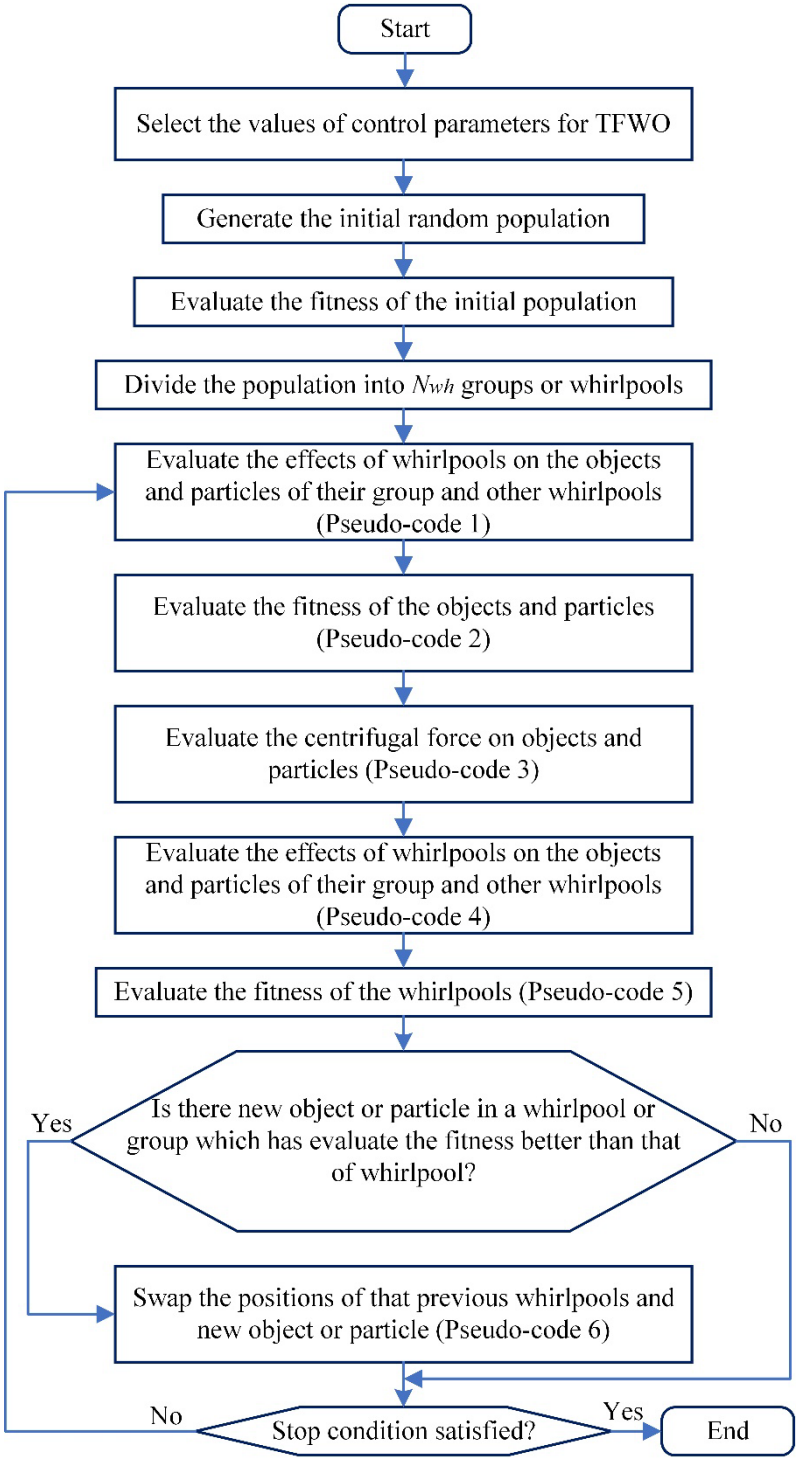

Figure 3. Flowchart of the original TFWO optimization algorithm.

3.2. The Proposed MTFWO

The initial iteration of the TFWO algorithm is inexperienced and produces inaccurate solutions to difficult optimization tasks. Although the TFWO protocol has its benefits, it also has certain shortcomings; this paper proposes a new MTFWO algorithm to address these issues and make information sharing more convenient for users.

With more people interacting from both populations, the search might come closer to the goal area without deciding on locally optimum answers. By more effectively searching the relevant decision space and improving exploitation capabilities, such an approach

greatly improves the TFWO algorithm's performance. The updated and enhanced search of the proposed MTFWO algorithm is described by Equation (38). Similar to the primary method, the equation incorporates a random coefficient and a sine and cosine coefficient that may be subtracted or added, as well as a local and global search. Due to the population's extended search area and the algorithm's ability to sidestep the local optimality trap, the global and local optimums are approached using distinct equations of motion and varying accelerations. To achieve this, we multiply it by random numbers, i.e., $rand + \left|cos\left(\delta_i^{\text{new}}\right) - sin\left(\delta_i^{\text{new}}\right)\right|$, which can change in the range from zero to two. This new equation greatly improves the recommended algorithm's ability to perform local and global searches and deal with a broad range of problems, and is shown by the following pseudocode 6:

$$\Delta X_i = \begin{cases} \left(rand + \left|cos\left(\delta_i^{\text{new}}\right) - sin\left(\delta_i^{\text{new}}\right)\right|\right) * \left(\left(\left(X_j + X_k\right) - 2 * X_i\right)\right); \text{ if } rand \le 0.25 \\ \left(1 + \left|cos\left(\delta_i^{\text{new}}\right) - sin\left(\delta_i^{\text{new}}\right)\right|\right) * \left(cos\left(\delta_i^{\text{new}}\right) * \left(Wh_f - X_i\right) - sin\left(\delta_i^{\text{new}}\right) * \left(Wh_w - X_i\right)\right); \text{ else} \end{cases} \tag{38}$$

$$X_i^{\text{new}} = Wh_j - \Delta X_i; \tag{39}$$

- Pseudocode 6:

  for $t = 1 : N_{Wh} - \{j\}$
  $\Delta_t = f(Wh_t) * |sum(Wh_t) - sum(X_i)|^{0.5}$
  end
  $Wh_f = Wh$ with a minimum value of Δ_t
  $Wh_w = Wh$ with a maximum value of Δ_t
  $\delta_i^{\text{new}} = \delta_i + rand_1 * rand_2 * \pi$
  if $rand \le 0.25$
  $\Delta X_i = (rand + |cos(\delta_i^{\text{new}}) - sin(\delta_i^{\text{new}})|) * \left(\left(\left(X_j + X_k\right) - 2 * X_i\right)\right);$
  else
  $\Delta X_i = (1 + |cos(\delta_i^{\text{new}}) - sin(\delta_i^{\text{new}})|) * \left(cos(\delta_i^{\text{new}}) * \left(Wh_f - X_i\right) - sin(\delta_i^{\text{new}}) * (Wh_w - X_i)\right);$
  $X_i^{\text{new}} = Wh_j - \Delta X_i;$
  end

As seen in the main equations of the TFWO, coefficient $\left(1 + \left|cos\left(\delta_i^{\text{new}}\right) - sin\left(\delta_i^{\text{new}}\right)\right|\right)$ takes a value between 1 and 2. However, this value should tend to zero for better algorithm searching and convergence performance in higher iterations. Since the proposed coefficient, i.e., $rand + \left|cos\left(\delta_i^{\text{new}}\right) - sin\left(\delta_i^{\text{new}}\right)\right|$, can take a value between 0 and 2, this shortcoming is fixed. According to (38), it is clear that the two terms *k* and *j* are added together, so to balance both sides of the subtraction sign and as a result of the general equation, the *i* term that is subtracted from these two terms must be multiplied by 2. This is a rule that is observed in almost all search algorithms. Of course, this equation can be written as follows:

Using (38) to increase the power of local search is the most important change made to the original algorithm. The value of 0.25 is chosen experimentally. It can balance between exploration and exploitation of the algorithm for the OPF problem. However, for other optimization problems, it should be appropriately adjusted.

4. MTFWO for Different OPF Problems

Both the TFWO and the MTFWO have been constructed on the IEEE 30 bus power system in order to solve the eight separate OPF issues that have been identified. The maximum number of TFWO and MTFWO iterations is 500 when *Npop* is equal to 33 and N_{Wh} is equal to 3 (population size and number of eddies, respectively). These are the power system parameters; they are found in [26]. On a computer furnished with an i7 CPU running at 3.0 GHz and 8 gigabytes of RAM, simulations were carried out using MATLAB 8.3. (R2014a).

4.1. OPF Solutions IEEE 30-Bus Network

What is seen in Figure 4 demonstrates this. OPF operation simulations are performed with an active load of 283.39 MW and a reactive load of 126.18 MVAr using the IEEE 30-bus test system. The essential parts of an IEEE 30-bus test system are as follows: The 41 lines of transmission include 9 shunt VAR compensators on buses 10, 12, 15, 17, 20, 21, 23, 24, and 29, and 4 off-nominal tap ratio transformers on lines 6–9, 6–10, 4–12, and 28–27.

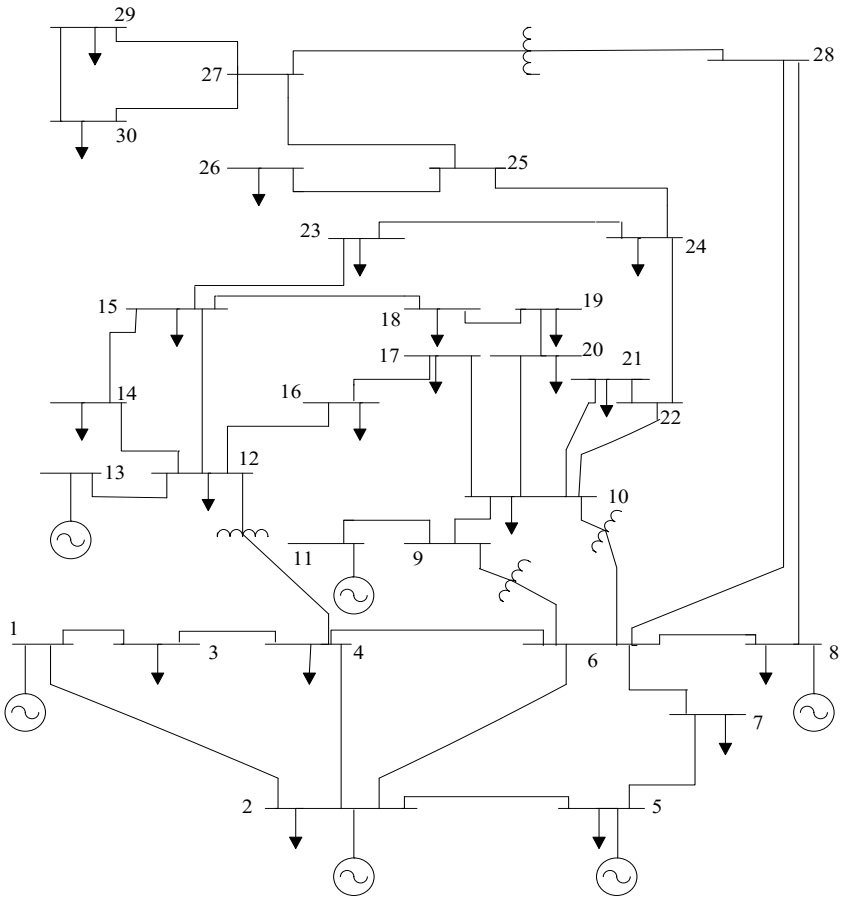

Figure 4. The layout of IEEE 30-bus network.

Buses 1, 2, 5, 8, 11, and 13 house the thermal power plants. Typical values for each parameter are 115 and 230 volts for generators, 0.95 and 1.1 p.u. for transformer tap settings, and 0 and 5 MVAr for shunt VAR compensations (0.95 and 1.1 p.u.). Load bus voltages may only be 0.95–1.05 p.u. in magnitude. To describe the nodes, buses, and heat generators that make up the system, this paper refers to the data supplied in reference [26].

Using the objective functions defined in Section 2, we first analyze the six deterministic OPF scenarios for the original setup of the system (without WT and PV) to show that the proposed MTFWO method is effective. Table 1 displays the best-case outcomes attained by the proposed MTFWO algorithm. The values shown here are the highest obtained throughout 30 iterations of testing each scenario. All the prerequisites have been met, and the results are consistent with the target functions that were considered. The MTFWO-derived optimal values for OPF variables are shown in Table 1 below, in the absence of stochastic renewable energy.

Table 1. Best solutions for six instances in the base case.

Decision Variables	Limitations		Instances					
	Lower	Upper	1	2	3	4	5	6
P_{G1} (MW)	49	251	177.1697	140.0001	198.7431	102.5856	176.3452	122.15643
P_{G2} (MW)	18	81	48.6955	55.0000	44.8830	55.5630	48.8217	52.54522
$P\,G_5$ (MW)	16	51	21.3899	24.0879	18.4621	38.1104	21.6363	31.52471
$P\,G_8$ (MW)	11	35	21.2389	34.9985	10.0000	35.0000	22.3212	35.00001
$P\,G_{11}$ (MW)	1	31	11.9284	18.3681	10.0001	30.0000	12.1560	26.77462
$P\,G_{13}$ (MW)	13	41	12.0000	17.6858	12.0002	26.6696	12.0000	20.98255
V_{G1}	0.965	1.11	1.0849	1.0744	1.0816	1.0698	1.0420	1.073036
V_{G2}	0.965	1.11	1.0607	1.0572	1.0580	1.0576	1.0227	1.057463
V_{G5}	0.965	1.11	1.0350	1.0313	1.0304	1.0359	1.0155	1.03283
V_{G8}	0.965	1.11	1.0383	1.0392	1.0373	1.0438	1.0076	1.04132
V_{G11}	0.965	1.11	1.0990	1.0876	1.0994	1.0830	1.0481	1.04022
V_{G13}	0.965	1.11	1.0513	1.0674	1.0636	1.0574	0.9874	1.02364
$T_{6–9}$	0.90	1.11	1.0721	1.0251	1.0415	1.0853	1.0696	1.10006
$T_{6–10}$	0.90	1.11	0.9185	0.9578	0.9701	0.9000	0.9000	0.95258
$T_{4–12}$	0.90	1.11	0.9762	1.0015	0.9951	0.9903	0.9415	1.03145
$T_{28–27}$	0.90	1.11	0.9738	0.9725	0.9780	0.9751	0.9710	1.00504
Q_{C10} (MVAR)	0.00	5.01	2.6670	4.8401	4.7382	4.5918	5.0000	3.38923
Q_{C12} (MVAR)	0.00	5.01	1.2027	0.0025	1.9409	0.1673	1.5141	0.06502
Q_{C15} (MVAR)	0.00	5.01	4.2890	3.0310	3.7691	4.4881	5.0000	3.92194
Q_{C17} (MVAR)	0.00	5.01	4.9995	4.9531	4.6145	5.0000	0	5.00006
Q_{C20} (MVAR)	0.00	5.01	4.2549	4.8434	4.3642	4.2338	5.0000	4.98046
Q_{C21} (MVAR)	0.00	5.01	4.9976	5.0000	5.0000	5.0000	5.0000	4.99994
Q_{C23} (MVAR)	0.00	5.01	3.3310	2.1912	2.9300	3.2521	5.0000	4.19076
Q_{C24} (MVAR)	0.00	5.01	4.9998	4.9990	5.0000	5.0000	5.0000	4.99966
Q_{C29} (MVAR)	0.00	5.01	2.6262	2.5173	2.6844	2.5592	2.6486	2.61303
Cost ($/h)	-	-	800.4781	646.4789	832.1666	859.0401	803.8125	830.34663
Emission (t/h)	-	-	0.3663	0.2835	0.4378	0.2289	0.3639	0.25293
Power losses (MW)	-	-	9.0222	6.7403	10.6885	4.5286	9.8804	5.58342
V.D.	-	-	0.9064	0.9193	0.8603	0.9274	0.0941	0.2983

4.1.1. Case 1: Minimization of Fuel Cost

In this scenario, we want to minimize the total fuel expense across all generators, as shown in Equation (40).

$$J_1 = \sum_{i=1}^{NG}\left(\alpha_i + b_i P_{Gi} + c_i P_{Gi}^2\right) + \lambda_P\left(P_{G1} - P_{G1}^{lim}\right)^2 + \lambda_Q \sum_{i=1}^{NG}\left(Q_{Gi} - Q_{Gi}^{lim}\right)^2 + \lambda_V \sum_{i=1}^{NL}\left(V_{Li} - V_{Li}^{lim}\right)^2 + \lambda_S \sum_{i=1}^{NTL}\left(S_{li} - S_{li}^{lim}\right)^2 \quad (40)$$

Based on experimental results in Table 2, the fuel cost using MTFWO is 800.4781 (USD/h) which is less in comparison to the optimization approaches in Table 2, which shows solutions using a variety of existing optimization methods, including a flower pollination algorithm (FPA) [26], MHBMO [20], hybrid shuffle frog leaping algorithm (SFLA) and simulated annealing (SFLA-SA) [27], hybrid modified particle swarm optimization (PSO) and SFLA (MPSO-SFLA) [28], hybrid phasor PSO (PPSO) and GSA (gravitational search algorithm) (PPSOGSA) [25], MSA [26], JAYA [29], firefly algorithm (FA) [30], manta ray foraging optimization (MRFO) [31], Aquila optimizer (AO) [32], adaptive real-coded biogeography-based optimization (ARCBBO) [33], hybrid of imperialist competitive algorithm (ICA) and TLBO (teaching-learning-based optimization) (MICA–TLA) [34], tabu search (TS) [35], artificial bee colony (ABC) [36], hybrid FA and JAYA (HFAJAYA) [30], hybrid PSO and GSA (PSOGSA) [37], modified Gaussian bare-bones ICA (MGBICA) [38], adaptive group search optimization (AGSO) [39], DE [40], moth-flame optimization (MFO) [26], evolutionary programming (EP) [41], GWO [14], stud krill herd algorithm (SKH) [42], and TFWO. Figure 5 shows the dramatic decrease in per-mile fuel costs.

Table 2. The obtained optimal results in the current works for Case 1.

Optimizer	Fuel Cost (USD/h)	Emmission (*t*/h)	Power Losses (MW)	V.D.
FPA [26]	802.7983	0.35959	9.5406	0.36788
MHBMO [20]	801.985	-	9.49	-
SFLA-SA [27]	801.79	-	-	-
MPSO-SFLA [28]	801.75	-	9.54	-
PPSOGSA [25]	800.528	-	9.02665	0.91136
MSA [26]	800.5099	0.36645	9.0345	0.90357
JAYA [29]	800.4794	-	9.06481	0.1273
FA [30]	800.7502	0.36532	9.0219	0.9205
MRFO [31]	800.7680	-	9.1150	-
AO [32]	801.83	-	-	-
ARCBBO [33]	800.5159	0.3663	9.0255	0.8867
MICA-TLA [34]	801.0488	-	9.1895	-
TS [35]	802.29	-	-	-
ABC [36]	800.660	0.365141	9.0328	0.9209
HFAJAYA [30]	800.4800	0.3659	9.0134	0.9047
PSOGSA [37]	800.49859	-	9.0339	0.12674
MGBICA [38]	801.1409	0.3296	-	-
AGSO [39]	801.75	0.3703	-	-
DE [40]	802.39	-	9.466	-
MFO [26]	800.6863	0.36849	9.1492	0.75768
EP [41]	803.57	-	-	-
GWO [14]	801.41	-	9.30	-
SKH [42]	800.5141	0.3662	9.0282	-
IEP [43]	802.46	-	-	-
TFWO	800.7308	0.3668	9.3207	0.9044
MTFWO	**800.4781**	0.3663	9.0222	0.9064

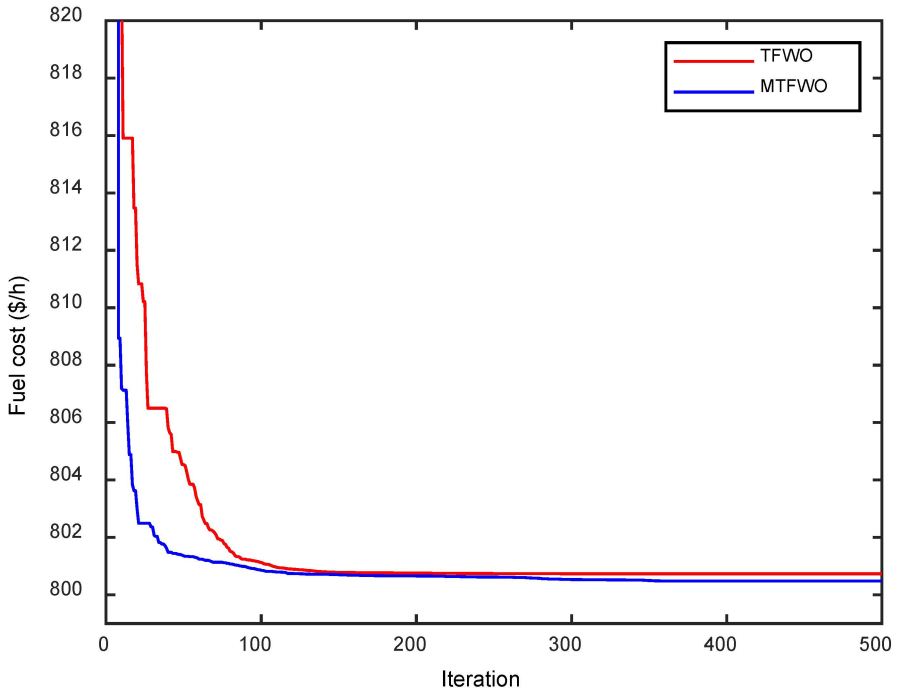

Figure 5. Convergence trends for Case 1.

4.1.2. Case 2: Minimization of Piecewise Quadratic Fuel Cost

There are a variety of fuel options that might be used to power thermal generating units in a power system, including oil, coal, and natural gas. This is due to the inherent

usefulness of the situation. Piecewise quadratic fuel cost functions may be derived for each fuel type by decomposing the overall fuel cost function of these units. Evidently, the fuel cost coefficients for the remaining single-fuel source generators are the same as in Instance 1. For the purpose of describing the fuel cost characteristics of the producing units connected to the first and second buses, a piecewise quadratic function is now utilized. Here is the formula for this function:

$$f_i(P_{Gi}) = \sum_{k=1}^{nf} \left(a_{i,k} + b_{i,k} P_{Gi} + c_{i,k} P_{Gi}^2 \right) \tag{41}$$

where $a_{i,k}$, $b_{i,k}$, and $c_{i,k}$ are coefficients for the cost of the ith power plant for the kth fuel choice, and n_f is the number of fossil fuel possibilities for the ith power plant.

The objective function can be described by Equation (42).

$$J_2 = \sum_{i=1}^{NG} f_i(P_{Gi}) + \lambda_P \left(P_{G1} - P_{G1}^{lim} \right)^2 + \lambda_Q \sum_{i=1}^{NG} \left(Q_{Gi} - Q_{Gi}^{lim} \right)^2 + \lambda_V \sum_{i=1}^{NL} \left(V_{Li} - V_{Li}^{lim} \right)^2 + \lambda_S \sum_{i=1}^{NTL} \left(S_{li} - S_{li}^{lim} \right)^2 \tag{42}$$

The simulation results are shown in Table 3 and demonstrate that the recommended approach results in a fuel cost of 646.4789 USD/h. The best fuel cost determined by the MTFWO algorithm is shown to be lower than the best fuel cost calculated by the sparrow search algorithm (SSA) [44], Lévy TLBO (LTLBO) [45], MFO [26], MICA-TLA [34], gbest guided ABC (GABC) [46], a modified DE (MDE) [40], social spider optimization (SSO) [47], FPA [26], MPSO-SFLA [28], an improved EP (IEP) [43], MSA [26], and TFWO in Table 3. In addition, the convergence of the proposed algorithms for the OPF problem at the cheapest feasible fuel cost is shown in Figure 6.

Table 3. The obtained optimal results in the current works for Case 2.

Optimizer	Fuel Cost (USD/h)	Emission (t/h)	Power Losses (MW)	V.D.
SSA [44]	646.7796	0.2836	6.5599	0.5320
LTLBO [45]	647.4315	0.2835	6.9347	0.8896
MFO [26]	649.2727	0.28336	7.2293	0.47024
MICA-TLA [34]	647.1002	-	6.8945	-
GABC [46]	647.03	-	6.8160	0.8010
MDE [40]	647.846	-	7.095	-
SSO [47]	663.3518	-	-	-
FPA [26]	651.3768	0.28083	7.2355	0.31259
MPSO-SFLA [28]	647.55	-	-	-
IEP [43]	649.312	-	-	-
MSA [26]	646.8364	0.28352	6.8001	0.84479
TFWO	646.9716	0.2838	6.7859	0.9099
MTFWO	646.4789	0.2835	6.7403	0.9193

4.1.3. Case 3: Minimization of Fuel Cost Considering Valve Point Effects (VPEs)

The effect of loading on the performance of the generators in the IEEE 30-bus test system may be simulated by adding a sinusoidal component to the cost curves of the generators; with the VPEs factored in, we obtain Equation (43).

$$\begin{aligned} J_3 = \sum_{i=1}^{NG} (\alpha_i + b_i P_{Gi} + c_i P_{Gi}^2) + \sum_{i=1}^{NG} |e_i \sin[f_i(P_{Gi}^{\min} - P_{Gi})]| + \lambda_P (P_{G1} - P_{G1}^{lim})^2 + \lambda_Q \sum_{i=1}^{NG} (Q_{Gi} - Q_{Gi}^{lim})^2 \\ + \lambda_V \sum_{i=1}^{NL} (V_{Li} - V_{Li}^{lim})^2 + \lambda_S \sum_{i=1}^{NTL} (S_{li} - S_{li}^{lim})^2 \end{aligned} \tag{43}$$

where e_i and f_i are the ith power plant's VPE costs.

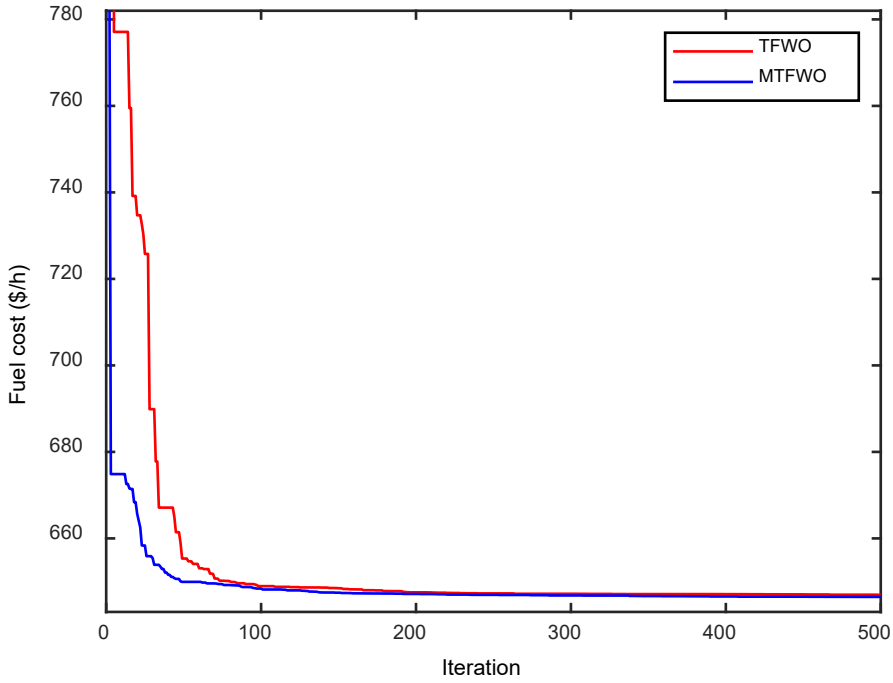

Figure 6. Convergence trends for Case 2.

The suggested MTFWO algorithm is compared to various heuristic techniques presented in the background section of the research in Table 4. In the tables can be found the optimal values for adjusting the control variables that were obtained using the proposed strategy. The simulation results showed that the recommended strategy resulted in the lowest feasible cost per hour for gasoline of USD 832.1666, which is a lower number when compared to the findings of other ways. The total amount spent on petrol fluctuated during the length of the research, as shown in Figure 7. Based on the data collected, it can be concluded that the offered MTFWO algorithm successfully identified appropriate OPF solutions for the conducted case study.

Table 4. The obtained optimal results in the current works for Case 3.

Optimizer	Fuel Cost (USD/h)	Emission (*t*/h)	Power Losses (MW)	V.D.
PSO [48]	832.6871	-	-	-
Self-adaptive penalty based on DE (SP-DE) [49]	832.4813	0.43651	10.6762	0.75042
FA [30]	832.5596	0.4372	10.6823	0.8539
HFAJAYA [30]	832.1798	0.4378	10.6897	0.8578
TFWO	832.6704	0.4380	10.8997	0.8365
MTFWO	832.1666	0.4378	10.6885	0.8603

We applied the recommended metaheuristics to the multiobjective OPF problems in the fourth through sixth examples, but we were unable to find a solution in any of them. Table 4 further summarizes the top solutions to the simulation findings for Cases 4–6 using the MTFWO method.

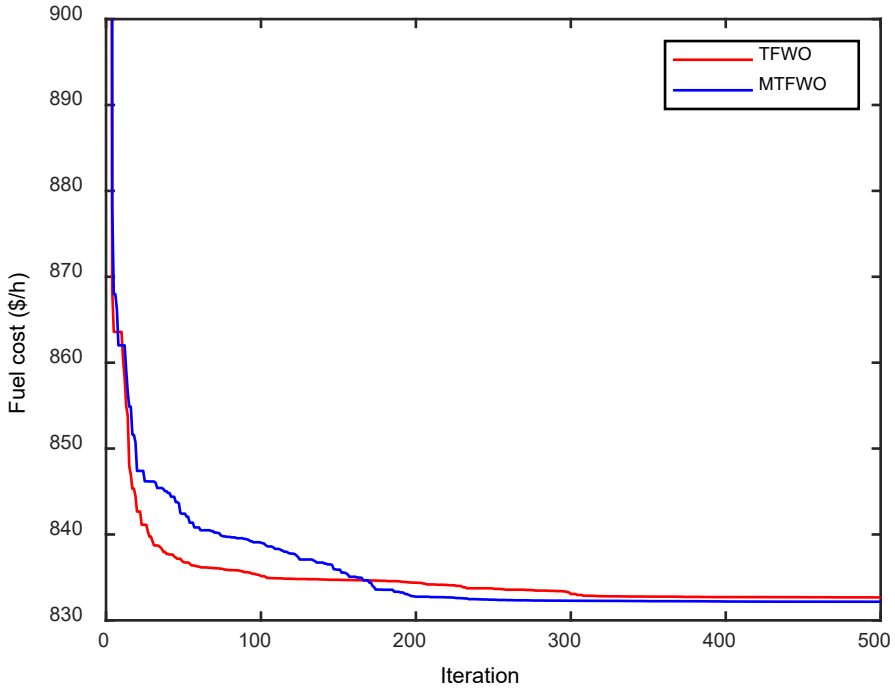

Figure 7. Convergence trends for Case 3.

4.1.4. Case 4: Minimization of Fuel Cost and Real Power Loss

The objective of this simulation technique for evaluating the MTFWO algorithm's performance is to minimize the active power losses and the quadratic cost function, which are respectively represented by Equations (16) and (17). As part of this simulation, we ran the MTFWO method to address the OPF problem 30 times.

The objective function is described by the following Equation (44):

$$J_4 = \sum_{i=1}^{NG}(\alpha_i + b_i P_{Gi} + c_i P_{Gi}^2) + \phi_p \sum_{ij} g_{ij}(V_i^2 + V_j^2 - 2V_i V_j cos\delta_{ij}) + \lambda_P (P_{G1} - P_{G1}^{lim})^2 + \lambda_Q \sum_{i=1}^{NG}(Q_{Gi} - Q_{Gi}^{lim})^2 + \lambda_V \sum_{i=1}^{NL}(V_{Li} - V_{Li}^{lim})^2 + \lambda_S \sum_{i=1}^{NTL}(S_{li} - S_{li}^{lim})^2 \quad (44)$$

where the value of ϕ_p is selected as 40, like [26].

Table 5 displays the simulation outcomes that were used to find the optimal values for changing the control variables. Figure 8 displays the study's convergence characteristic of the best fuel cost result obtained from the algorithms, and Table 5 compares the proposed MTFWO algorithm to heuristic strategies found in the literature. The MTFWO algorithm yielded optimum fuel costs of 859.0401 USD per hour and active power losses of 4.5286 (MW). Based on the data in Table 5, it is obvious that the MTFWO algorithm produces a substantially lower estimate of the total objective function compared to the best result obtained in the aforementioned body of research.

4.1.5. Case 5: Minimization of Fuel Cost and V.D.

The bus's voltage is a crucial indicator of reliability and safety. Solutions to OPF difficulties that are centered on costs may be theoretically achievable, but their voltage profiles may not be suitable. A dual-target function is required here to simultaneously increase fuel economy and enhance voltage profile by limiting load bus voltage deviations from 1.0 per unit. In certain cases, it is possible to express the objective function mathematically (45).

$$J_5 = \sum_{i=1}^{NG}(\alpha_i + b_i P_{Gi} + c_i P_{Gi}^2) + \phi_v \sum_{i=1}^{NPQ}|V_i - 1.0| + \lambda_P (P_{G1} - P_{G1}^{lim})^2 + \lambda_Q \sum_{i=1}^{NG}(Q_{Gi} - Q_{Gi}^{lim})^2 + \lambda_V \sum_{i=1}^{NL}(V_{Li} - V_{Li}^{lim})^2 + \lambda_S \sum_{i=1}^{NTL}(S_{li} - S_{li}^{lim})^2 \quad (45)$$

where ϕ_v was given the value of 100 [26] as a factor. Finding the best answer to the issue has been a focus of the suggested approach. Table 6 displays the results of using the MTFWO method to determine the best settings for the control parameters. Additionally, the results of the comparison are shown in Table 6; from this, it is obvious that the MTFWO greatly decreased this multiobjective function. In Figure 9, we can see the convergence curve for this multiobjective function, as computed by the TFWO and MTFWO algorithms for the Case 5 problem.

Table 5. The obtained optimal results in the current works for Case 4.

Optimizer	Fuel Cost (USD/h)	Emission (*t*/h)	Power Losses (MW)	V.D.	J_4
Enhanced MSA (EMSA) [50]	859.9514	0.2278	4.6071	0.7758	1044.2354
Quasi-oppositional modified Jaya (QOMJaya) [51]	826.9651	-	5.7596	-	1402.9251
Modified Jaya (MJaya) [51]	827.9124	-	5.7960	-	1059.7524
Multiobjective ant lion algorithm (MOALO) [52]	826.4556	0.2642	5.7727	1.2560	1057.3636
Spherical prune DE (SpDEA) [53]	837.8510	-	5.6093	0.8106	1062.223
MSA [26]	859.1915	0.2289	4.5404	0.92852	1040.8075
TFWO	859.3726	0.2290	4.5498	0.9188	1041.3646
MTFWO	859.0401	0.2289	4.5286	0.9274	**1040.1841**

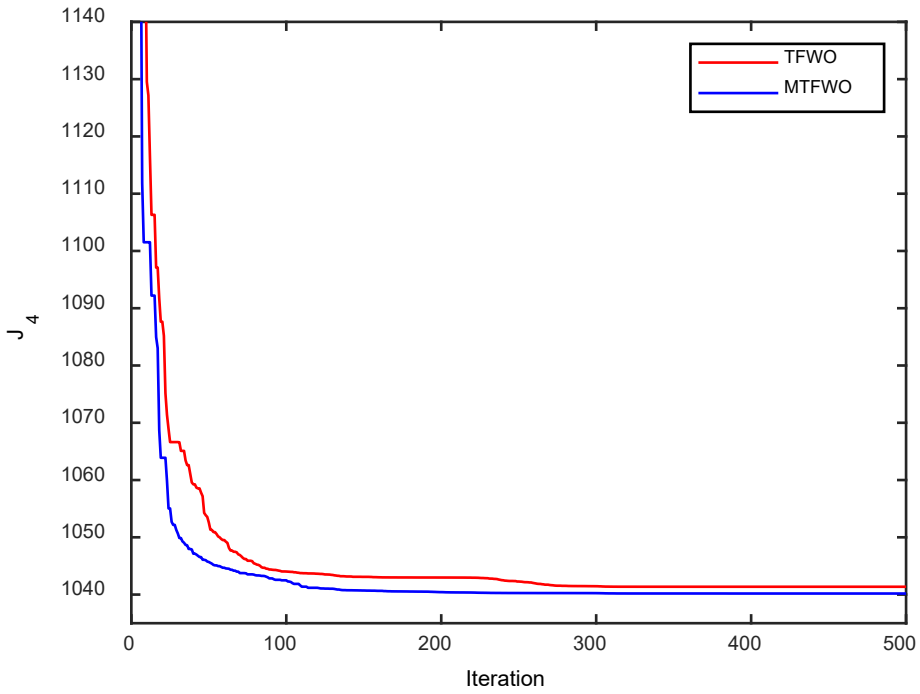

Figure 8. Convergence trends for Case 4.

Table 6. The obtained optimal results in the current works for Case 5.

Optimizer	Fuel Cost (USD/h)	Emission (*t*/h)	Power Losses (MW)	V.D.	J_5
Dragonfly algorithm (DA) with aging PSO (DA-APSO) [54]	802.63	-	-	0.1164	814.2700
SpDEA [53]	803.0290	-	9.0949	0.2799	831.0190
Multiobjective modified bare-bones PSO (BB-MOPSO) [55]	804.9639	-	-	0.1021	815.1739
MPSO [26]	803.9787	0.3636	9.9242	0.1202	815.9987
EMSA [50]	803.4286	0.3643	9.7894	0.1073	814.1586
Hybrid PSO and salp swarm Optimization (PSO-SSO) [56]	803.9899	0.367	9.961	0.0940	813.3899
Multiobjective modified ICA (MOMICA) [55]	804.9611	0.3552	9.8212	0.0952	814.4811
MFO [26]	803.7911	0.36355	9.8685	0.10563	814.3541
TFWO [1]	803.416	0.365	9.795	0.101	813.5160
Salp swarm Optimization (SSO) [56]	803.73	0.365	9.841	0.1044	814.1700
PSO [56]	804.477	0.368	10.129	0.126	817.0770
Modified sorting nongenetic algorithm (MNSGA-II) [55]	805.0076	-	-	0.0989	814.8976
TFWO	803.9968	0.3641	10.1240	0.0995	813.9468
MTFWO	803.8125	0.3639	9.8804	0.0941	**813.2225**

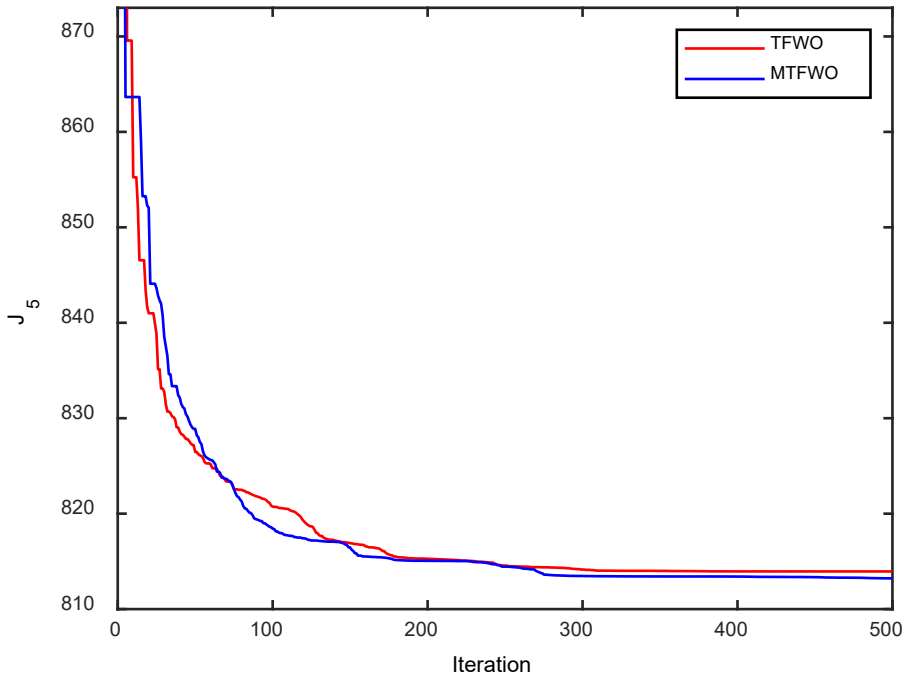

Figure 9. Convergence trends for Case 5.

4.1.6. Case 6: Minimization of Fuel Cost, Emissions, V.D., and Losses

The function for lowering emissions linked to the OPF issue may be thought of as the total of all the many kinds of emissions that are examined, including SOX and NOX, with a proper price or weighting placed on each pollutant that is released. We want to minimize fuel cost, V.D., emission, and power loss while taking into account two major groups of emissions gases using the total objective function, provided by Equation (46).

$$J_6 = J_5 + \phi_p \sum_{ij} g_{ij}(V_i^2 + V_j^2 - 2V_iV_j\cos\delta_{ij}) + \phi_e \sum_{i=1}^{NG}\left(\alpha_i + \beta_i P_{Gi} + \gamma_i P_{Gi}^2 + \xi_i \exp(\theta_i P_{Gi})\right) \quad (46)$$

In (46), the weighting factors with values of $\phi_v = 21$, $\phi_p = 22$, and $\phi_e = 19$ are employed to strike a balance among the problem's various goals (see [26] for details). The optimal settings for the controls are shown in Table 7 for Case 6. This demonstrates that the OPF issue can be solved most efficiently using the MTFWO technique. The best fuel cost result achieved by the MTFWO algorithm is compared to those found by other methods in Table 7. Objective function values reported in the literature are lower than the lowest value recorded here, i.e., 964.2606. Just take a glance at the desk to see the end product. The convergence curve for the global objective function in Case 6 was calculated using TFWO and MTFWO (Figure 10).

Table 7. The obtained optimal results in the current works for Case 6.

Algorithm	Fuel Cost (USD/h)	Emission (*t*/h)	Power Losses (MW)	V.D.	J_6
Hybrid Jaya–Powell's pattern search 2 (J-PPS2) [57]	830.8672	0.2357	5.6175	0.2948	965.1201
MOALO [52]	826.2676	0.2730	7.2073	0.7160	1005.0512
BB-MOPSO [55]	833.0345	0.2479	5.6504	0.3945	970.3379
PSO [56]	828.2904	0.261	5.644	0.55	968.9674
Hybrid Jaya–Powell's pattern search 3 (J-PPS3) [57]	830.3088	0.2363	5.6377	0.2949	965.0228
MSA [26]	830.639	0.25258	5.6219	0.29385	965.2907
MNSGA-II [55]	834.5616	0.2527	5.6606	0.4308	972.9429
Hybrid Jaya–Powell's pattern search 1 (J-PPS1) [57]	830.9938	0.2355	5.6120	0.2990	965.2159
Multiobjective DA (MODA) [58]	828.49	0.265	5.912	0.585	975.8740
MFO [26]	830.9135	0.25231	5.5971	0.33164	965.8080
Improved NSGA-II (I-NSGA-III) [59]	881.9395	0.2209	4.7449	0.1754	994.2078
SSO [56]	829.978	0.25	5.426	0.516	964.9360
TFWO	830.5073	0.2535	5.6410	0.2987	965.6985
MTFWO	830.3466	0.2529	5.5834	0.2983	**964.2508**

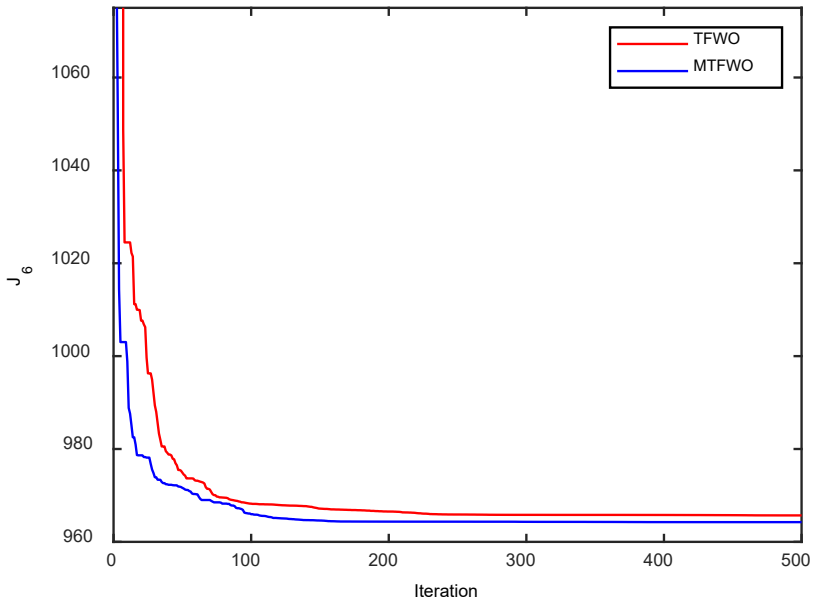

Figure 10. Convergence trends for Case 6.

4.2. Solving the OPF Problem Considering WT and PV Generation

4.2.1. Case 7: Minimization of the Generation Cost Incorporating WT and PV Generation

For a system that makes use of renewable sources such as WT and PV, reducing the fuel cost, wind cost, and PV cost indicated by Equation (47) is the goal.

$$J_7 = J_1 + \sum_{i}^{NW} Fcost(WT_i) + \sum_{i}^{NPV} Fcost(PV_i) \quad (47)$$

This, together with the values for work temperature and photovoltaic power, may be obtained in the aforementioned equation. WT_i represents the cost of the ith thermal generator to produce the electrical energy, whereas PV_i stands for the cost of the ith solar photovoltaic generator. Table 8 shows the specifications of wind power and solar PV plants' PDFs [60]. In Table 8, the PDF parameters and the cost coefficients are identical to those found in Case 1. The best results produced by the proposed MTFWO method are shown in Table 9.

Table 8. Specifications of the WT and PV plants' PDFs.

	WT Plants				PV Plant		
Wind Farm	**No. of Turbines**	**Rated Power, P_{wr} (MW)**	**Weibull PDF Parameters**	**Weibull Mean, Mwbl**	**Rated Power, P_{sr} (MW)**	**Lognormal PDF Parameters**	**Lognormal Mean, Mlgn**
1 (bus 5)	25	75	$c = 9, k = 2$	$v = 7.976$ m/s	50 (bus 13)	$\mu = 6, \sigma = 0.6$	$G = 483$ W/m^2
2 (bus 11)	20	60	$c = 10, k = 2$	$v = 8.862$ m/s			

Table 9. The variables optimal values obtained for Case 7.

Variables	**TFWO**	**MTFWO**
P_{G1} (MW)	134.90791	134.90791
P_{G2} (MW)	29.1694	27.5152
P_{ws1} (MW)	44.1115	43.1911
P_{G3} (MW)	10	10
P_{ws2} (MW)	37.2235	36.4806
P_{ss} (MW)	33.755	37.096
V_{G1}	1.0718	1.0714
V_{G2}	1.0569	1.0564
V_{G5}	1.035	1.0344
V_{G8}	1.0612	1.0975
V_{G11}	1.0997	1.1
V_{G13}	1.0487	1.0497
Q_{G1} (MVAR)	−2.29534	−2.4284
Q_{G2} (MVAR)	11.8338	11.6775
Q_{ws1} (MVAR)	22.42	22.4327
Q_{G3}(MVAR)	40	40
Q_{ws2} (MVAR)	30	30
Q_{ss} (MVAR)	15.0431	15.3694
Fuelvlvcost (USD/h)	442.7995	437.3083
Wind gen cost (USD/h)	248.4581	242.7311
Solar gen cost (USD/h)	91.2925	101.8322
Total cost (USD/h)	782.5501	**781.8715**
Emission (t/h)	1.76192	0.45530
Power losses (MW)	5.7673	5.7908
V.D.	0.45386	0.45530

The presented figures represent the best results from 30 repetitions of each test. All requirements have been satisfied, and the outcomes are in line with the intended uses. With the aforementioned control variables fine-tuned, the overall fuel cost for Case 7 was drastically lowered in comparison to the first run of the TFWO algorithm. A contrast

between the convergence characteristics of TFWO and MTFWO for Case 7 is shown in Figure 11.

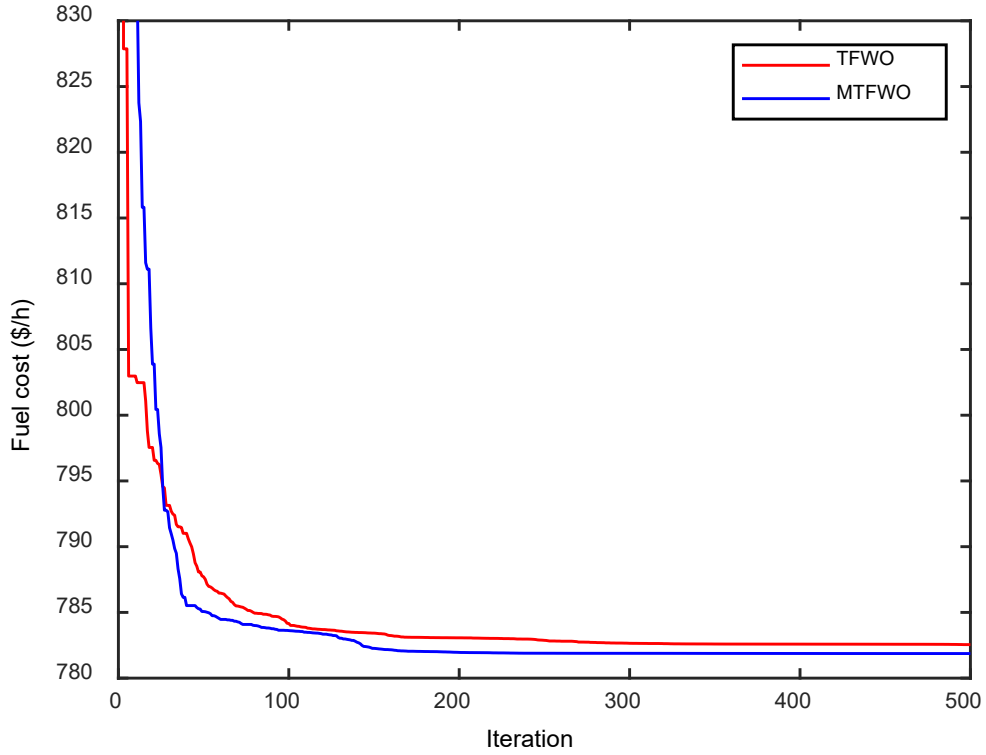

Figure 11. Convergence trends for Case 7.

4.2.2. Case 8: Minimization of the Generation Cost Incorporating WT and PV Generation with the Carbon Tax

C_{tax}, short for the carbon tax, is charged on the production of carbon dioxide and other greenhouse gases with the intention of increasing financing for renewable energy sources such as WT and PV. An approximate cost for carbon emissions may be calculated using the following formula [60]:

$$C_E = C_{tax} E \tag{48}$$

$$J_8 = J_7 + C_{tax} E \tag{49}$$

Approximately 20 USD per ton in C_{tax} is predicted [60]. Table 10 displays OPF results as estimated by the carbon price and anticipated output of wind turbines and solar generators. Table 10 shows that the quality and stability of solutions achieved with the suggested MTFWO are improved over those obtained with the traditional TFWO approach. There is an increase in the penetration of wind and solar electricity in comparison to Case 7 if a carbon price is contemplated (Case 8) and imposed (Case 7). Furthermore, Figure 12 displays the convergence qualities of these distinct approaches. Compared to traditional TFWO, there is little question that the suggested MTFWO yields superior solutions and converges to the faster optimal solution. Taking into account stochastic aspects such as WT and PV productions, these statistics demonstrate that MTFWO can handle very complex OPF situations.

Table 10. Case 8's ideal values for all variables.

Variables	TFWO	MTFWO
P_{G1} (MW)	124.05273	123.42123
P_{G2} (MW)	34.5467	32.7675
P_{ws1} (MW)	46.79	45.8762
P_{G3} (MW)	10	10
P_{ws2} (MW)	39.3703	38.6302
P_{ss} (MW)	33.9203	37.9805
V_{G1}	1.071	1.0705
V_{G2}	1.0576	1.057
V_{G5}	1.0365	1.0359
V_{G8}	1.0405	1.0404
V_{G11}	1.0981	1.0982
V_{G13}	1.0548	1.0562
Q_{G1} (MVAR)	−2.54117	−2.69805
Q_{G2} (MVAR)	12.4645	12.2864
Q_{ws1} (MVAR)	22.9406	22.9691
Q_{G3}(MVAR)	35.4423	35.2379
Q_{ws2} (MVAR)	30	30
Q_{ss} (MVAR)	17.3678	17.8613
Fuelvlvcost (USD/h)	435.9284	428.3159
Wind gen cost (USD/h)	265.5061	259.5920
Solar gen cost (USD/h)	91.5097	104.5964
Total cost (USD/h)	792.9442	792.5043
Emission (t/h)	0.91868	0.88611
J_8	811.3178	810.2265
Power losses (MW)	5.2800	5.2756
V.D.	0.46700	0.46966
Carbon tax (USD/h)	18.3736	17.7222

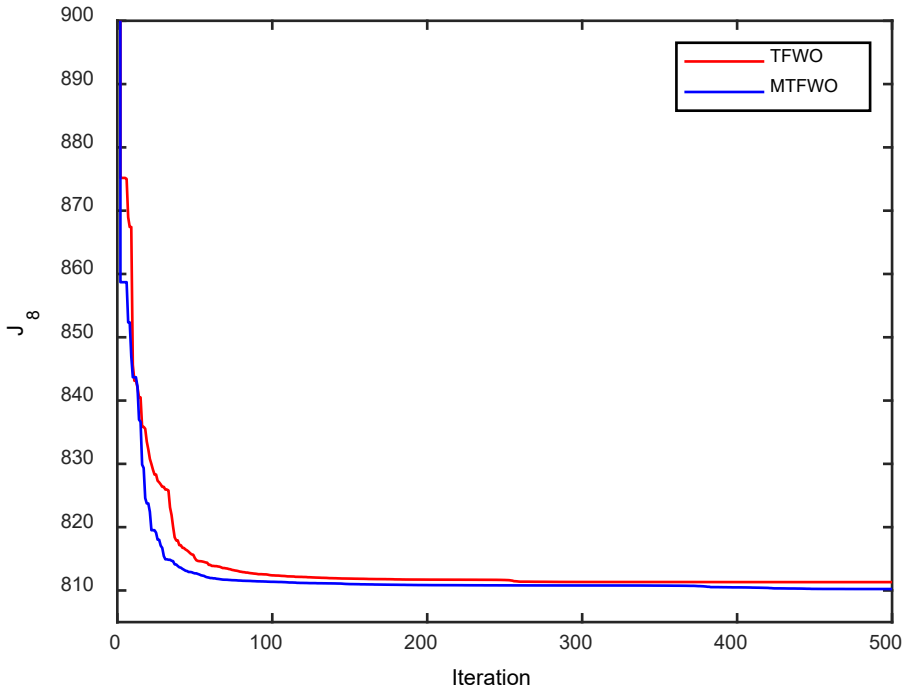

Figure 12. Convergence trends for Case 8.

4.3. Discussions

Table 11 shows side-by-side comparisons of all the results, including the least (Min), average (Mean), greatest (Max), and standard deviation (Std.) of expenditures, as well as the time required for simulation. Compared to the TFWO approach, the suggested

MTFWO excels in every conceivable way, as shown in Table 11. TFWO's best-case scenario is also inferior to the worst-case scenario described for the MTFWO; these comparisons demonstrate the possibility for the suggested MTFWO to provide a workable solution to the OPF issue. The consistency and robustness of the suggested method's findings are shown by the proximity of the best, average, and worst solutions of the MTFWO. The given data suggest that the suggested approach may converge to a nearly global optimal state in a realistic amount of time.

Table 11. Statistical results to show the performance of algorithms.

Method	Min	Mean	Max	Std.	Time (s)
			Case 1		
TFWO	800.7308	800.9731	801.4006	0.49	28
MTFWO	**800.4781**	**800.5693**	**800.7024**	**0.12**	28
			Case 2		
TFWO	646.9716	647.2543	647.6081	0.31	28
MTFWO	**646.4789**	**646.5545**	**646.6870**	**0.14**	28
			Case 3		
TFWO	832.6704	832.9429	833.3842	0.54	28
MTFWO	**832.1666**	**832.2869**	**832.4130**	**0.16**	28
			Case 4		
TFWO	1041.3646	1041.7019	1042.1275	0.45	27
MTFWO	**1040.1841**	**1040.2748**	**1040.5255**	**0.27**	28
			Case 5		
TFWO	813.9468	814.2870	814.5443	0.33	28
MTFWO	**813.2225**	**813.3611**	**813.4389**	**0.11**	28
			Case 6		
TFWO	965.6985	965.9988	966.4672	0.50	28
MTFWO	**964.2508**	**964.4095**	**964.5010**	**0.17**	27
			Case 7		
TFWO	782.5501	782.8716	783.3426	0.52	31
MTFWO	**781.8715**	**781.9663**	**782.2456**	**0.25**	31
			Case 8		
TFWO	811.3178	811.6268	811.9747	0.39	31
MTFWO	**810.2265**	**810.3940**	**810.4835**	**0.12**	31

5. Conclusions

The multiobjective OPF has become one of the most popular optimization problems in the power systems sector. Our study proposes a modified optimization strategy for OPF-related challenges. This optimization is based on the water's surface optimization technique (TFWO) with a modified TFWO, known as a modified turbulent flow (MTFWO). Initially, OPF was formulated as a nonlinear optimization problem with equality and inequality constraints, to be solved inside existing power systems. Throughout the course of the investigation, many goal functions were considered. Included were a quadratic cost function, a piecewise quadratic cost function, and a cost function that took into account the valve point impact of an IEEE 30-bus test system with integrated WT and PV generators. The objective was to raise the voltage profile while simultaneously decreasing transmission line and bus expenses. In short, this paper presented the OPF problem, which considers all constraints related to the generators, and this indicates that this paper can observe as comprehensive research in the OPF sector. The proposed MTFWO was shown to be resilient, computationally efficient, and adaptive for handling the OPF problem with multiple objective functions. Simulation results indicated that the suggested technique may

identify optimum settings for the test system's control variables. The suggested MTFWO algorithm gave higher-quality solutions to OPF problems than stochastic approaches. To show this, the results obtained with MTFWO were compared to those obtained with the other methodologies outlined. Results from the simulation also proved the effectiveness of the proposed method in real-world circumstances. The suggested metaheuristic performed better than a number of commonly utilized and potent algorithms that had previously been published. This demonstrates the effectiveness and utility of the suggested metaheuristic in handling problems involving several goals concurrently. This paper has shown the advantages of the MTFWO method in order to achieve the set of optimal solutions and the best compromise solution to OPF problems, respectively. The proposed paradigm proved to be a useful tool for tackling a wide variety of challenges related to the global characteristics of very complex systems.

Funding: The author extends their appreciation to the deputyship for Research & Innovation, Ministry of Education in Saudi Arabia for funding this research work through the project number (IFP-2020-93).

Institutional Review Board Statement: Not applicable.

Informed Consent Statement: Not applicable.

Data Availability Statement: Not applicable.

Acknowledgments: The author extends their appreciation to the deputyship for Research & Innovation, Ministry of Education in Saudi Arabia for funding this research work through the project number (IFP-2020-93).

Conflicts of Interest: The author declares no conflict of interest.

References

1. Sarhan, S.; El-Sehiemy, R.; Abaza, A.; Gafar, M. Turbulent Flow of Water-Based Optimization for Solving Multiobjective Technical and Economic Aspects of Optimal Power Flow Problems. *Mathematics* **2022**, *10*, 2106. [CrossRef]
2. Kahraman, H.T.; Akbel, M.; Duman, S. Optimization of Optimal Power Flow Problem Using Multi-Objective Manta Ray Foraging Optimizer. *Appl. Soft Comput.* **2022**, *116*, 108334. [CrossRef]
3. Ngoko, B.O.; Sugihara, H.; Funaki, T. Optimal Power Flow Considering Line-Conductor Temperature Limits under High Penetration of Intermittent Renewable Energy Sources. *Int. J. Electr. Power Energy Syst.* **2018**, *101*, 255–267. [CrossRef]
4. Baccoli, R.; Frattolillo, A.; Mastino, C.; Curreli, S.; Ghiani, E. A Comprehensive Optimization Model for Flat Solar Collector Coupled with a Flat Booster Bottom Reflector Based on an Exact Finite Length Simulation Model. *Energy Convers. Manag.* **2018**, *164*, 482–507. [CrossRef]
5. Baccoli, R.; Kumar, A.; Frattolillo, A.; Mastino, C.; Ghiani, E.; Gatto, G. Enhancing Energy Production in a PV Collector–Reflector System Supervised by an Optimization Model: Experimental Analysis and Validation. *Energy Convers. Manag.* **2021**, *229*, 113774. [CrossRef]
6. Morshed, M.J.; Hmida, J.B.; Fekih, A. A Probabilistic Multiobjective Approach for Power Flow Optimization in Hybrid Wind-PV-PEV Systems. *Appl. Energy* **2018**, *211*, 1136–1149. [CrossRef]
7. Mura, P.G.; Baccoli, R.; Innamorati, R.; Mariotti, S. An Energy Autonomous House Equipped with a Solar PV Hydrogen Conversion System. *Energy Procedia* **2015**, *78*, 1998–2003. [CrossRef]
8. Momoh, J.A.; El-Hawary, M.E.; Adapa, R. A Review of Selected Optimal Power Flow Literature to 1993. II. Newton, Linear Programming and Interior Point Methods. *IEEE Trans. Power Syst.* **1999**, *14*, 105–111. [CrossRef]
9. Momoh, J.A.; Adapa, R.; El-Hawary, M.E. A Review of Selected Optimal Power Flow Literature to 1993. I. Nonlinear and Quadratic Programming Approaches. *IEEE Trans. Power Syst.* **1999**, *14*, 96–104. [CrossRef]
10. Pourakbari-Kasmaei, M.; Mantovani, J.R.S. Logically Constrained Optimal Power Flow: Solver-Based Mixed-Integer Nonlinear Programming Model. *Int. J. Electr. Power Energy Syst.* **2018**, *97*, 240–249. [CrossRef]
11. Ben Hmida, J.; Javad Morshed, M.; Lee, J.; Chambers, T. Hybrid Imperialist Competitive and Grey Wolf Algorithm to Solve Multiobjective Optimal Power Flow with Wind and Solar Units. *Energies* **2018**, *11*, 2891. [CrossRef]
12. Boussa\"\id, I.; Lepagnot, J.; Siarry, P. A Survey on Optimization Metaheuristics. *Inf. Sci.* **2013**, *237*, 82–117. [CrossRef]
13. Abdo, M.; Kamel, S.; Ebeed, M.; Yu, J.; Jurado, F. Solving Non-Smooth Optimal Power Flow Problems Using a Developed Grey Wolf Optimizer. *Energies* **2018**, *11*, 1692. [CrossRef]
14. Niknam, T.; Narimani, M.R.; Aghaei, J.; Tabatabaei, S.; Nayeripour, M. Modified Honey Bee Mating Optimisation to Solve Dynamic Optimal Power Flow Considering Generator Constraints. *IET Gener. Transm. Distrib.* **2011**, *5*, 989. [CrossRef]
15. Salkuti, S.R. Optimal Power Flow Using Multi-Objective Glowworm Swarm Optimization Algorithm in a Wind Energy Integrated Power System. *Int. J. Green Energy* **2019**, *16*, 1547–1561. [CrossRef]

16. Kumari, B.A.; Vaisakh, K. Integration of Solar and Flexible Resources into Expected Security Cost with Dynamic Optimal Power Flow Problem Using a Novel DE Algorithm. *Renew. Energy Focus* **2022**, *42*, 48–69. [CrossRef]
17. Ali, Z.M.; Aleem, S.H.E.A.; Omar, A.I.; Mahmoud, B.S. Economical-Environmental-Technical Operation of Power Networks with High Penetration of Renewable Energy Systems Using Multi-Objective Coronavirus Herd Immunity Algorithm. *Mathematics* **2022**, *10*, 1201. [CrossRef]
18. Avvari, R.K.; DM, V.K. A Novel Hybrid Multi-Objective Evolutionary Algorithm for Optimal Power Flow in Wind, PV, and PEV Systems. *J. Oper. Autom. Power Eng.* **2022**, *11*, 130–143.
19. Ahmad, M.; Javaid, N.; Niaz, I.A.; Almogren, A.; Radwan, A. A Bio-Inspired Heuristic Algorithm for Solving Optimal Power Flow Problem in Hybrid Power System. *IEEE Access* **2021**, *9*, 159809–159826. [CrossRef]
20. El-Fergany, A.A.; Hasanien, H.M. Single and Multiobjective Optimal Power Flow Using Grey Wolf Optimizer and Differential Evolution Algorithms. *Electr. Power Components Syst.* **2015**, *43*, 1548–1559. [CrossRef]
21. Srithapon, C.; Fuangfoo, P.; Ghosh, P.K.; Siritaratiwat, A.; Chatthaworn, R. Surrogate-Assisted Multi-Objective Probabilistic Optimal Power Flow for Distribution Network with Photovoltaic Generation and Electric Vehicles. *IEEE Access* **2021**, *9*, 34395–34414. [CrossRef]
22. Duman, S.; Li, J.; Wu, L. AC Optimal Power Flow with Thermal–Wind–Solar–Tidal Systems Using the Symbiotic Organisms Search Algorithm. *IET Renew. Power Gener.* **2021**, *15*, 278–296. [CrossRef]
23. Elattar, E.E. Optimal Power Flow of a Power System Incorporating Stochastic Wind Power Based on Modified Moth Swarm Algorithm. *IEEE Access* **2019**, *7*, 89581–89593. [CrossRef]
24. Ghasemi, M.; Davoudkhani, I.F.; Akbari, E.; Rahimnejad, A.; Ghavidel, S.; Li, L. A Novel and Effective Optimization Algorithm for Global Optimization and Its Engineering Applications: Turbulent Flow of Water-Based Optimization (TFWO). *Eng. Appl. Artif. Intell.* **2020**, *92*, 103666. [CrossRef]
25. Ullah, Z.; Wang, S.; Radosavljević, J.; Lai, J. A Solution to the Optimal Power Flow Problem Considering WT and PV Generation. *IEEE Access* **2019**, *7*, 46763–46772. [CrossRef]
26. Mohamed, A.-A.A.; Mohamed, Y.S.; El-Gaafary, A.A.M.; Hemeida, A.M. Optimal Power Flow Using Moth Swarm Algorithm. *Electr. Power Syst. Res.* **2017**, *142*, 190–206. [CrossRef]
27. Niknam, T.; Narimani, M.R.; Jabbari, M.; Malekpour, A.R. A Modified Shuffle Frog Leaping Algorithm for Multiobjective Optimal Power Flow. *Energy* **2011**, *36*, 6420–6432. [CrossRef]
28. Narimani, M.R.; Azizipanah-Abarghooee, R.; Zoghdar-Moghadam-Shahrekohne, B.; Gholami, K. A Novel Approach to Multi-Objective Optimal Power Flow by a New Hybrid Optimization Algorithm Considering Generator Constraints and Multi-Fuel Type. *Energy* **2013**, *49*, 119–136. [CrossRef]
29. Warid, W.; Hizam, H.; Mariun, N.; Abdul-Wahab, N. Optimal Power Flow Using the Jaya Algorithm. *Energies* **2016**, *9*, 678. [CrossRef]
30. Alghamdi, A.S. A Hybrid Firefly–JAYA Algorithm for the Optimal Power Flow Problem Considering Wind and Solar Power Generations. *Appl. Sci.* **2022**, *12*, 7193. [CrossRef]
31. Guvenc, U.; Bakir, H.; Duman, S.; Ozkaya, B. Optimal Power Flow Using Manta Ray Foraging Optimization. In Proceedings of the International Conference on Artificial Intelligence and Applied Mathematics in Engineering, Antalya, Turkey, 18–20 April 2020; pp. 136–149.
32. Khamees, A.K.; Abdelaziz, A.Y.; Eskaros, M.R.; El-Shahat, A.; Attia, M.A. Optimal Power Flow Solution of Wind-Integrated Power System Using Novel Metaheuristic Method. *Energies* **2021**, *14*, 6117. [CrossRef]
33. Ramesh Kumar, A.; Premalatha, L. Optimal Power Flow for a Deregulated Power System Using Adaptive Real Coded Biogeography-Based Optimization. *Int. J. Electr. Power Energy Syst.* **2015**, *73*, 393–399. [CrossRef]
34. Ghasemi, M.; Ghavidel, S.; Rahmani, S.; Roosta, A.; Falah, H. A Novel Hybrid Algorithm of Imperialist Competitive Algorithm and Teaching Learning Algorithm for Optimal Power Flow Problem with Non-Smooth Cost Functions. *Eng. Appl. Artif. Intell.* **2014**, *29*, 54–69. [CrossRef]
35. Abido, M.A. Optimal Power Flow Using Tabu Search Algorithm. *Electr. Power Components Syst.* **2002**, *30*, 469–483. [CrossRef]
36. Abaci, K.; Yamacli, V. Differential Search Algorithm for Solving Multiobjective Optimal Power Flow Problem. *Int. J. Electr. Power Energy Syst.* **2016**, *79*, 1–10. [CrossRef]
37. Radosavljević, J.; Klimenta, D.; Jevtić, M.; Arsić, N. Optimal Power Flow Using a Hybrid Optimization Algorithm of Particle Swarm Optimization and Gravitational Search Algorithm. *Electr. Power Components Syst.* **2015**, *43*, 1958–1970. [CrossRef]
38. Ghasemi, M.; Ghavidel, S.; Ghanbarian, M.M.; Gitizadeh, M. Multi-Objective Optimal Electric Power Planning in the Power System Using Gaussian Bare-Bones Imperialist Competitive Algorithm. *Inf. Sci.* **2015**, *294*, 286–304. [CrossRef]
39. Hazra, J.; Sinha, A.K. A Multiobjective Optimal Power Flow Using Particle Swarm Optimization. *Eur. Trans. Electr. Power* **2011**, *21*, 1028–1045. [CrossRef]
40. Sayah, S.; Zehar, K. Modified Differential Evolution Algorithm for Optimal Power Flow with Non-Smooth Cost Functions. *Energy Convers. Manag.* **2008**, *49*, 3036–3042. [CrossRef]
41. Sood, Y. Evolutionary Programming Based Optimal Power Flow and Its Validation for Deregulated Power System Analysis. *Int. J. Electr. Power Energy Syst.* **2007**, *29*, 65–75. [CrossRef]
42. Pulluri, H.; Naresh, R.; Sharma, V. A Solution Network Based on Stud Krill Herd Algorithm for Optimal Power Flow Problems. *Soft Comput.* **2018**, *22*, 159–176. [CrossRef]

43. Ongsakul, W.; Tantimaporn, T. Optimal Power Flow by Improved Evolutionary Programming. *Electr. Power Components Syst.* **2006**, *34*, 79–95. [CrossRef]
44. Jebaraj, L.; Sakthivel, S. A New Swarm Intelligence Optimization Approach to Solve Power Flow Optimization Problem Incorporating Conflicting and Fuel Cost Based Objective Functions. *e-Prime-Adv. Electr. Eng. Electron. Energy* **2022**, *2*, 100031.
45. Ghasemi, M.; Ghavidel, S.; Gitizadeh, M.; Akbari, E. An Improved Teaching–Learning-Based Optimization Algorithm Using Lévy Mutation Strategy for Non-Smooth Optimal Power Flow. *Int. J. Electr. Power Energy Syst.* **2015**, *65*, 375–384. [CrossRef]
46. Roy, R.; Jadhav, H.T. Optimal Power Flow Solution of Power System Incorporating Stochastic Wind Power Using Gbest Guided Artificial Bee Colony Algorithm. *Int. J. Electr. Power Energy Syst.* **2015**, *64*, 562–578. [CrossRef]
47. Nguyen, T.T. A High Performance Social Spider Optimization Algorithm for Optimal Power Flow Solution with Single Objective Optimization. *Energy* **2019**, *171*, 218–240. [CrossRef]
48. Bouchekara, H.R.E.H.; Chaib, A.E.; Abido, M.A.; El-Sehiemy, R.A. Optimal Power Flow Using an Improved Colliding Bodies Optimization Algorithm. *Appl. Soft Comput.* **2016**, *42*, 119–131. [CrossRef]
49. Biswas, P.P.; Suganthan, P.N.; Mallipeddi, R.; Amaratunga, G.A.J. Optimal Power Flow Solutions Using Differential Evolution Algorithm Integrated with Effective Constraint Handling Techniques. *Eng. Appl. Artif. Intell.* **2018**, *68*, 81–100. [CrossRef]
50. Bentouati, B.; Khelifi, A.; Shaheen, A.M.; El-Sehiemy, R.A. An Enhanced Moth-Swarm Algorithm for Efficient Energy Management Based Multi Dimensions OPF Problem. *J. Ambient Intell. Humaniz. Comput.* **2020**, *12*, 9499–9519. [CrossRef]
51. Warid, W.; Hizam, H.; Mariun, N.; Abdul Wahab, N.I. A Novel Quasi-Oppositional Modified Jaya Algorithm for Multi-Objective Optimal Power Flow Solution. *Appl. Soft Comput.* **2018**, *65*, 360–373. [CrossRef]
52. Herbadji, O.; Slimani, L.; Bouktir, T. Optimal Power Flow with Four Conflicting Objective Functions Using Multiobjective Ant Lion Algorithm: A Case Study of the Algerian Electrical Network. *Iran. J. Electr. Electron. Eng.* **2019**, *15*, 94–113. [CrossRef]
53. Ghoneim, S.S.M.; Kotb, M.F.; Hasanien, H.M.; Alharthi, M.M.; El-Fergany, A.A. Cost Minimizations and Performance Enhancements of Power Systems Using Spherical Prune Differential Evolution Algorithm Including Modal Analysis. *Sustainability* **2021**, *13*, 8113. [CrossRef]
54. Shilaja, C.; Ravi, K. Optimal Power Flow Using Hybrid DA-APSO Algorithm in Renewable Energy Resources. *Energy Procedia* **2017**, *117*, 1085–1092. [CrossRef]
55. Ghasemi, M.; Ghavidel, S.; Ghanbarian, M.M.; Gharibzadeh, M.; Azizi Vahed, A. Multi-Objective Optimal Power Flow Considering the Cost, Emission, Voltage Deviation and Power Losses Using Multiobjective Modified Imperialist Competitive Algorithm. *Energy* **2014**, *78*, 276–289. [CrossRef]
56. El Sehiemy, R.A.; Selim, F.; Bentouati, B.; Abido, M.A. A Novel Multi-Objective Hybrid Particle Swarm and Salp Optimization Algorithm for Technical-Economical-Environmental Operation in Power Systems. *Energy* **2020**, *193*, 116817. [CrossRef]
57. Gupta, S.; Kumar, N.; Srivastava, L.; Malik, H.; Pliego Marugán, A.; García Márquez, F.P. A Hybrid Jaya—Powell's Pattern Search Algorithm for Multi-Objective Optimal Power Flow Incorporating Distributed Generation. *Energies* **2021**, *14*, 2831. [CrossRef]
58. Ouafa, H.; Linda, S.; Tarek, B. Multi-Objective Optimal Power Flow Considering the Fuel Cost, Emission, Voltage Deviation and Power Losses Using Multiobjective Dragonfly Algorithm. In Proceedings of the International Conference on Recent Advances in Electrical Systems, Hammamet, Tunusia, 22–24 December 2017.
59. Zhang, J.; Wang, S.; Tang, Q.; Zhou, Y.; Zeng, T. An Improved NSGA-III Integrating Adaptive Elimination Strategy to Solution of Many-Objective Optimal Power Flow Problems. *Energy* **2019**, *172*, 945–957. [CrossRef]
60. Biswas, P.P.; Suganthan, P.N.; Amaratunga, G.A.J. Optimal Power Flow Solutions Incorporating Stochastic Wind and Solar Power. *Energy Convers. Manag.* **2017**, *148*, 1194–1207. [CrossRef]